ANNEALING HEAT TREATMENT OF ORGANIC MATERIAL FOR CONTROLLED BULK HETEROJUNCTION SOLAR CELLS

BY

OLALEKAN DEBORAH OLUBUNMI

A THESIS

SUBMITTED TO THE AFRICAN UNIVERSITY OF SCIENCE AND TECHNOLOGY

ABUJA – NIGERIA

IN PARTIAL FULFILLMENT OF THE REQUIREMENTS FOR THE

AWARD OF MASTER OF SCIENCE IN (DEPARTMENT OF MATERIALS SCIENCE AND ENGINEERING)

SUPERVISOR: PROF. WOLE SOBOYEJO

MAY, 2013

ANNEALING HEAT TREATMENT OF ORGANIC MATERIAL FOR CONTROLLED BULK HETEROJUNCTION SOLAR CELLS

A THESIS APPROVED

BY

SUPERVISOR: _____
PROF. WOLE SOBOYEJO

MEMBER: _____
DR. ZEBAZE KANA

MEMBER: _____
DR. SHOLA ODUSANYA

DEDICATION

This thesis is dedicated to my darling husband Oyewole Oluwaseun Kehinde

ACKNOWLEDGEMENT

First and foremost, I wish to render my sincere and unalloyed appreciation to my supervisor Prof. Wole Soboyejo for his guidance, understanding, patience, encouragement and advice he has provided throughout the course of this thesis. Without his untiring guidance and persistent help, this thesis would not have been possible. During the most difficult times he has given me moral support to move on. I have been extremely lucky to have him as my supervisor; he is not just a supervisor but a father and an inspiration in many ways. May God bless you abundantly!

I also express my deepest appreciation to my committee members Dr. Zebaze Kana and Dr. Shola Odusanya for their enormous help through my career path. I thank them for their guidance, valuable advice, encouraging words and personal attention for the success of my programme at AUST. They kept me going from the very beginning and gave me constant support. I equally thank Dr. A.A. Oberafo, the Director of Research, Physics Advanced laboratory for permitting me to undergo my Msc. Study and also for making it possible for equipments to be available to undertake my research. I say a big thank you

I use this opportunity to sincerely acknowledge the AUST-SHESTCO-PRINCETON-STEPB project for the financial assistance in the form of travel fellowship which enabled me to carry out major part of my research work. I am also indebted to all the members of Soboyejo research group: Dr Karen Malatesta, Tiffany Tong, Onobu Akogwu, Jing Du, for their attention and care while in Princeton. Your generosity and patience will forever be remembered.

I equally like to appreciate Mr. Jerry Poirier of Princeton Institute for the Science and Technology of Materials (PRISM) for the invaluable help and assistance rendered with the use of scanning electron microscope (SEM) to get meaningful results. Thank you for your time and effort.

My heartfelt gratitude goes to all my colleagues in Physics Advanced Laboratory, Sheda Science and Technology Complex (SHESTCO), Abuja. Your support and motivation has made me forge ahead in my academic pursuit.

I cannot but say a big “THANK YOU” to all my colleagues at AUST especially my classmates in Materials Science and Engineering stream: Ifeanyi, Elijah, Taiwo, Funsho, Sharafadeen, Owoseni, Amine, Odette, Bimbo and Fortunatus. You guys have been wonderful and made my stay at AUST to be a memorable one. My sincere gratitude also goes to my research group in AUST (Energy group) for their inputs and constructive criticism especially the AMRS president, AUST chapter, Mr. Benjamin Agjei-Tuffour.

I owe a lot to my parents, Mr & Mrs Olalekan for their encouragement, prayers and help at every stage of my personal and academic life. My deep appreciation also goes to my siblings: Mrs Aderemi Koku, Samuel, Grace, Joseph, Esther and Rhoda for their love and words of encouragement.

At this point, I like to express my profound gratitude to my darling husband, Oyewole Oluwaseun Kehinde for his unconditional love and continued support. There are no enough words to express my heartfelt appreciation for always encouraging me to pursue my dreams. Your encouragement and support has provided me with strength to complete this task

Above all, I owe it all to almighty God for giving me life to see the completion of this thesis and granting me wisdom, knowledge, understanding and the strength to undertake this research successfully.

ABSTRACT

The morphology of active layers of organic solar cells plays crucial roles in achieving good performing devices with longer life span. The process of fabricating these devices involved post deposition thermal annealing, which increases the crystallinity and enhances phase-separated domains of deposited active layer components. A blended composite of regioregular poly(3-hexylthiophene) (P3HT) and phenyl-C61-butyric acid methyl ester (PCBM) is used as the active layer in this BHJ solar cell. In this work, the blends were prepared for different ratio of P3HT: PCBM and annealed at different temperatures. A variety of experimental techniques were employed to observe the microstructures of various active layers at different domains after quenching to room temperature. A better understanding of the correlation between the observed microstructures and electrical characteristic of the active layers is therefore used to explain the performance of organic solar cells.

TABLE OF CONTENTS

LIST OF FIGURES

LIST OF TABLES

CHAPTER 1

INTRODUCTION

1.1 INTRODUCTION

The ever increasing demand for electricity around the globe has led scientists into developing a renewable, sustainable, cheap and stable source of energy. Solar cells are able to meet some of these needs by converting energy from sunlight to electrical energy. Solar energy has a great potential to generate power because the earth receives about $1.2\ X\ 10^{17}\ W$ of solar power [1]. This is enough to meet the daily energy demands of the ever increasing world population in less than an hour. The need for efficient, stable, and low cost solar energy is proving to be more imperative. [2]

Although, conventional silicon solar cells are well established and reasonably efficient, [3] they are relatively expensive to produce for low income earners. Also, the scarcity of some of the elements required to make solar grade silicon [4] is another major obstacle that makes silicon solar cells to be non-sustainable. Hence, new materials and novel solar technologies are being developed in an effort to produce cheaper and more sustainable sources of power using solar energy [5].

Electrical power can be generated from incident electromagnetic irradiation using organic photovoltaic (OPV) materials. Essentially, organic solar cells (OPVs) provide us with a range of benefits such as flexibility, light weight, lower cost of production and fast processing. The major challenges of OPV cells are their relatively low efficiency (~8% compared to ~10%-20% for silicon solar cells) and their limited stability under working conditions compared to their inorganic counterparts. The active layer, consisting of electron donor and acceptor is where the energy conversion from solar energy to electrical energy occurs. The processing, deposition and annealing of this active layer plays a major role in contributing to the overall efficiency of OPVs.

Prior work has shown that mixtures of poly (3-hexylthiophene) and phenyl-C61-butyric acid

methyl ester (P3HT: PCBM) provide the highest levels of solar energy conversion when used as the active layer in organic solar cells [6]. In fact, almost every world record in the efficiency of such solar cells has been achieved by changing the P3HT: PCBM ratio and microstructure. Such mixtures can promote charge hopping that gives rise to the improved charge mobility in nanostructured films with well controlled distributions of PCBM in the matrices of P3HT. In a way to further improve the overall performance of the organic solar cells, the right post deposition annealing temperature of the active layer is a priority [7]. Furthermore, a nanostructured film (Figure 1b) of organic active layer has greater absorption spectrum that commensurate the solar emission spectrum [8]. Nanostructured film of P3HT: PCBM can retain the solar emission spectrum compared to thin smooth film (Figure 1b). Thus, ways of improving the efficiency of these solar cells through control of the microstructure as well as the architecture of these active layers are thoroughly studied in this thesis.

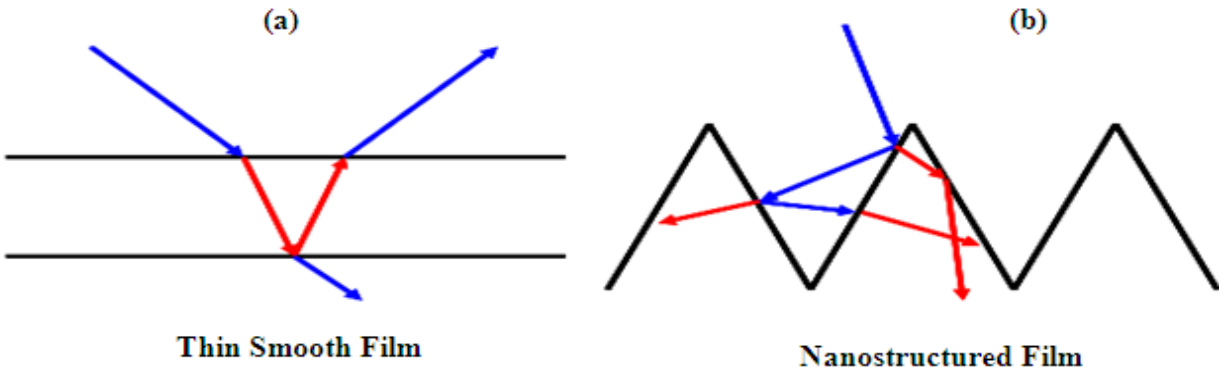

Figure 1.1: Structures of Thin Films (a) Smooth (b) Nanostructured

1.2 AIMS AND OBJECTIVES

This thesis will explore the effects of well controlled P3HT: PCBM mixtures on the microstructure and electrical/ optical properties of P3HT: PCBM bulk heterojunction (BHJ) layers. A range of nanostructured microstructures will be produced by the annealing of P3HT: PCBM mixtures. Metastable far-from–equilibrium structures will also be produced by quenching and tempering

treatments. The electrical and optical properties of these layers will be measured before measuring the current-voltage characteristics of the BHJ devices with well controlled compositions and microstructures.

The research will be carried out in various steps as follows;

- Preparation of P3HT:PCBM solution in ratio 1:0.8 by weight
- Sputtering of anodic layer (transparent conducting oxide) on glass
- Spin coating of PEDOT: PSS solution on ITO-coated glass followed by deposition of the prepared active layers.
- Checking of the thicknesses of deposited layers using surface profiler.
- Annealing or quenching and tempering of the deposited active layers at different temperatures.
- Observation of surface morphology of the layers using Scanning Electron Microscope
- Thermal deposition of cathodic electrode using thermal evaporator
- Measurements of Current-Voltage characteristics of the devices.

1.3 OUTLINE OF THE THESIS

Following introduction in chapter one, a detailed background and literature review is presented in chapter two. This will be followed by chapter three in which the experimental procedures will be described. The results obtained from the studies of microstructure and electrical/optical properties will be presented in Chapter four before summarizing the salient conclusions from this work and presenting suggestions for future work in chapter five.

1.4 REFERENCES

[1] Jenna de Boisblanc; Synthesis and Characterization of P3HT:PCBM Organic Solar Cells, May 2010

[2] René Janssen, Introduction to polymer solar cells, Eindhoven University of Technology, The

Netherlands (3Y280)

[3] B. A. Sandén, Materials Availability for Thin-Film PV and the Need for ‘Technodiversity’, at the EUROPV 2003 Conference 2003, Bologna (Spain).

[4] Chetan Kamble, D. R. Mehta; Organic Solar Technique using P3HT and PCBM as Promising Materials, *International Journal of Engineering Research and Applications Vol. 3, Issue 1, January -February 2013, pp.2024-2028*

[5] Carr, Chen, Elshobaki, Mahadevapuram and Chaudhary Controlling nanomorphology in plastic solar cells, Nanomaterials and Energy Volume 1 Issue NME1

[6] Serap Günes, Organic Solar Cells and Their Nanostructural Improvement, *Energy Efficiency and Renewable Energy Through Nanotechnology*, (London Limited: Springer-Verlag, 2011) 171-225.

CHAPTER 2

BACKGROUND AND LITERATURE REVIEW

2.1 ORGANIC SOLAR CELLS

Photovoltaics can be grouped into two major classes namely inorganic PV and organic PV, depending on the active materials used for their production. Currently, the active materials used for the production of inorganic photovoltaic are materials such as silicon, gallium arsenide (GaAs), Cadmium Telluride (CdTe), etc. However, other alternative active materials include conjugated polymers and molecules, which are generally, bulk heterojunction systems for the new frontier organic solar cells.

Conjugated polymers are organic materials that consist of alternating single and double bonds [1]. In conjugated materials, three sp^2 hybrid orbitals form covalent bonds, one with each of the carbon atoms next to it, and the third with a hydrogen atom or other group. The remaining electron occupies a p_z orbital. The common overlap of p_z orbitals creates π bonds along the conjugated backbone, by delocalizing π electrons along the entire conjugated path. These π bonds are the origin of the conducting properties of polymers. The highest filled (π) orbital is named the highest occupied molecular orbital (HOMO) and the empty lowest (π^*) orbital is named the lowest unoccupied molecular orbital (LUMO). The energy gap structure (Figures 2.2 and 2.3) between the HOMO and the LUMO ranges from 1 to 4 eV [36], which makes most semiconducting polymers ideally suited for applications in optoelectronic devices operating in the visible light range [2]. The typical structure of a conjugated polymer is shown below in Figure 2.1.

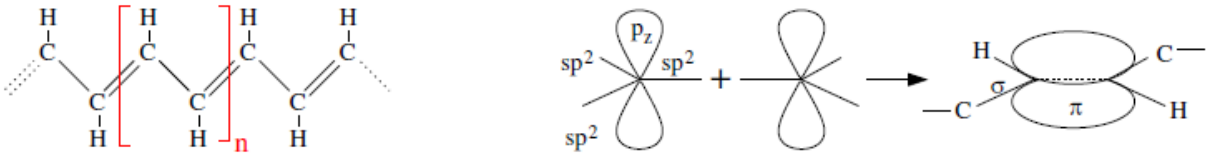

Figure 2.1: (a) Chemical structure of Polymers (b) formation of the delocalized π bonds along the polymer chain (right) from the p_z orbitals when adding polymer repetition units

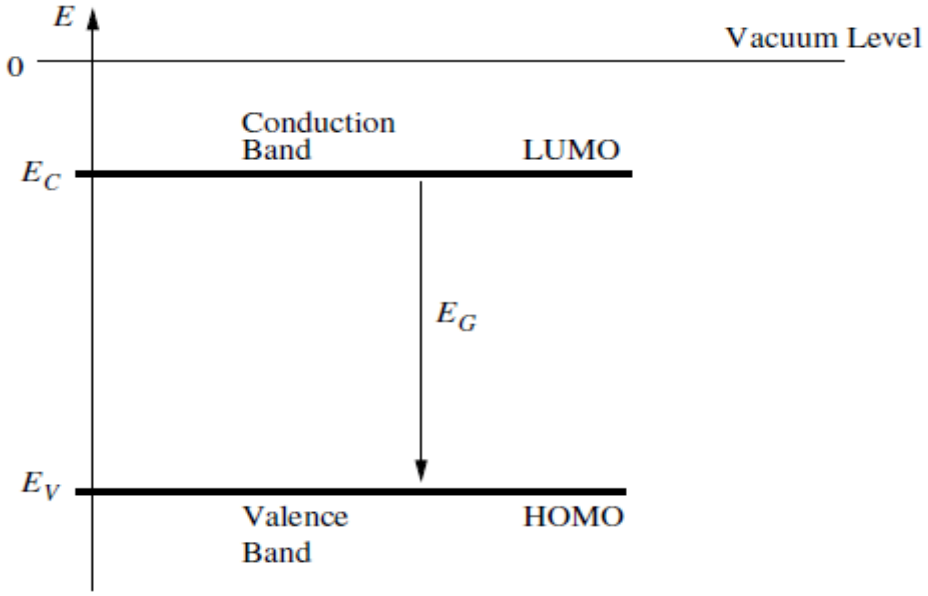

Figure 2.2: Energy Band Gap Structure of a Buck Heterojunction System

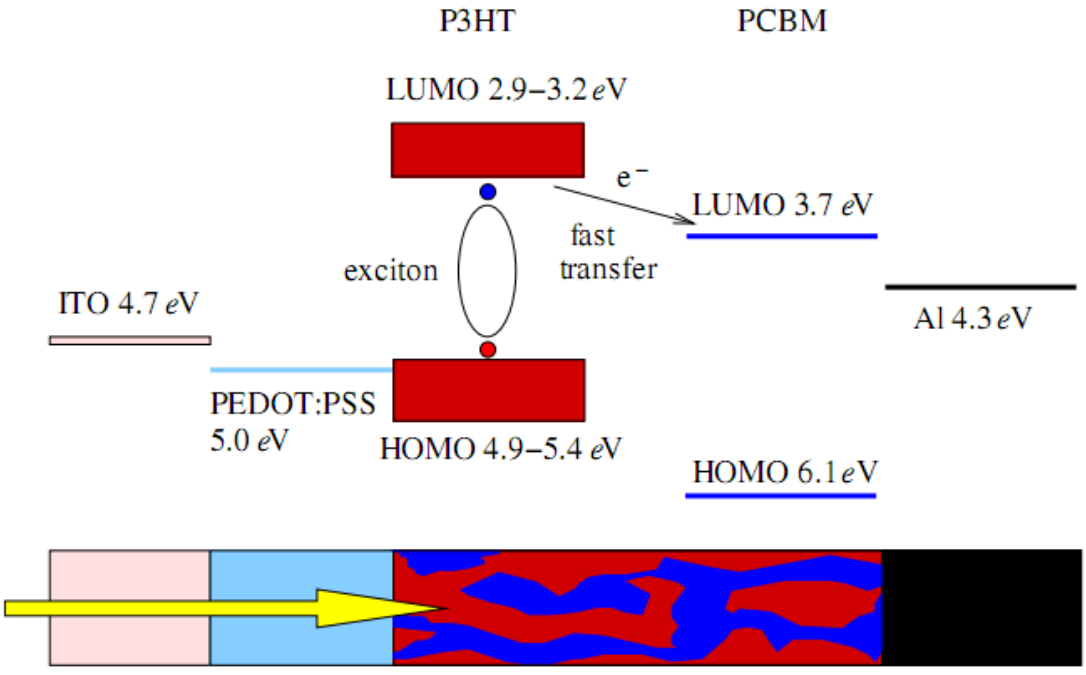

Figure 2.3: The complete energy scheme for P3HT: PCBM based organic solar cells. (Adapted from Ref 3)

An organic solar cell is made up of a photoactive layer sandwiched between two electrodes of different work functions. One of the electrodes is transparent, while the other one in not. Sunlight passes through the transparent electrode and therefore high transmittance is needed to promote generation of exciton.

The possibility of chemically manipulating the materials properties of the polymers (such as band gap, molecular weight, energy levels and structural order) as well as the ease and lower cost of processing techniques has attracted a lot of attention [37]. The lower cost of production can be achieved by the use of fabrication processes [47,48,49]. One of these techniques is spin coating. The latest developments in ink-jet printing, micro-contact printing, as well as other soft lithography techniques, have further improved the potential of conjugated polymers for low-cost fabrication of large-area integrated devices on both rigid and flexible substrates.

The field of conjugated materials-based electronics started in 1977 when Heeger et al. [22] discovered that the conductivity of the conjugated polymer polyacetylene can be increased by seven orders of magnitude upon oxidation with iodine. They won the Nobel Prize in Chemistry [5-8]. This discovery led, subsequently, to the discovery of electroluminescence in a poly(p-phenylene vinylene) by Burroughes et al. [9,10].

2.2 GENERAL OPERATING PRINCIPLE OF ORGANIC SOLAR CELLS

For a successful organic solar cell, four essential processes have to be optimized to attain a high conversion efficiency of solar energy into electrical energy. First, incident photons are absorbed onto the active layer, consisting of an electron donor and acceptor of a reasonable thickness, on the order of nm [38]. The absorption spectrum of the active layer must match that of the solar emission spectrum in order to harvest as many photons as possible [39].

Following the absorption of light, electron-hole pairs (also referred to as excitons) are generated and diffused into an active interface. However, for an efficient solar cell, all excitons

have to reach the photo-active interface within the exponential lifetime (τ_{exc}). They must also reach the interface without recombination by covering a distance (L_{exc}). The distance covered by excitons to reach the bulk heterojunction interface is given by [40]:

$$L_{exc} = \sqrt{D_{exc} \times \tau_{exc}} \tag{2.1}$$

where D_{exc} is the diffusion coefficient of the excitons.

The next step is the separation of the electron-hole pairs into electrons and holes. These will then be collected at the electrodes, a transparent conducting oxide such as Indium Tin Oxide (ITO) on one side and a metal contact at the other side [11]. For a working device, the two photoactive materials are sandwiched between two metal electrodes of different work functions. This is done in order to collect the created charges, as shown below in Figure 2.4.

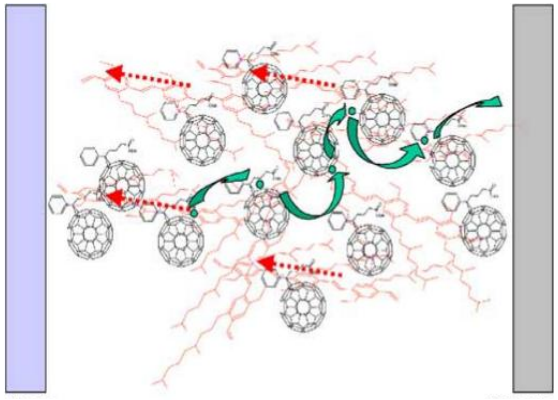

Figure 2.4: Sandwiched Bulk Heterojunction Active Material Between an ITO and a Metal

2.2.1 Absorption of light

In semiconductors, near-infrared to ultraviolet absorption is due to band-to-band transitions in these materials. Once a photon is absorbed, its energy excites an electron within the material, which is promoted from the ground state to an excited state [12]. In this process, energy is conserved, and the energy of photon absorbed is equal to the difference in energy

between the initial and final electronic states. In the case of inorganic semiconductors, once a photon is absorbed, an electron is excited from the valence band to the conduction band in a σ – σ* transition [41]. Since σ bonded atomic orbitals interact strongly, energy bands in inorganic crystals are wide [13]. The σ bonds are formed when energy level of atomic orbitals split and become overlapped, giving rise to the band structure in inorganic crystals. On the other hand, for organic molecules, absorption takes place through $\pi - \pi^*$ transitions.

The absorption of a photon principally leads to the creation of a strongly bound singlet exciton, due to overlap of molecular orbital and the low dielectric constant ($\epsilon_r \approx 3 - 4$) of organic semi-conductors, compared to most inorganic semiconductors with dielectric constants ($\epsilon_r > 10$). Thus, excitons have Coulombic binding energies, ranging from about 100 MeV to about 1 eV [14].

2.2.2 Formation and Separation of Charges

Organic solar cells have much lower dielectric constants than their inorganic counterparts [38]. As a result of this, their thermal energy at room temperature is not sufficient to dissociate photo-generated electron-hole pairs. Therefore, a heterojunction is required for charge separation to be feasible. A heterojunction is an interface that is formed between two materials (the electron donor and electron acceptor) due to the difference in their electron affinities and ionization potentials [22]. The photo-generated exciton has a strong binding energy (>0.1eV) [42] and dissociation into free charge carriers is very unlikely in either donor material or acceptor material alone.

However, the fact that both materials have two energy levels that are separated by an energy gap promotes the efficient dissociation of excitons. Hence, when the exciton in the donor material diffuses to the interface of the heterojunction, an electron is transferred to the acceptor material, thereby splitting the exciton into its constituent charges.

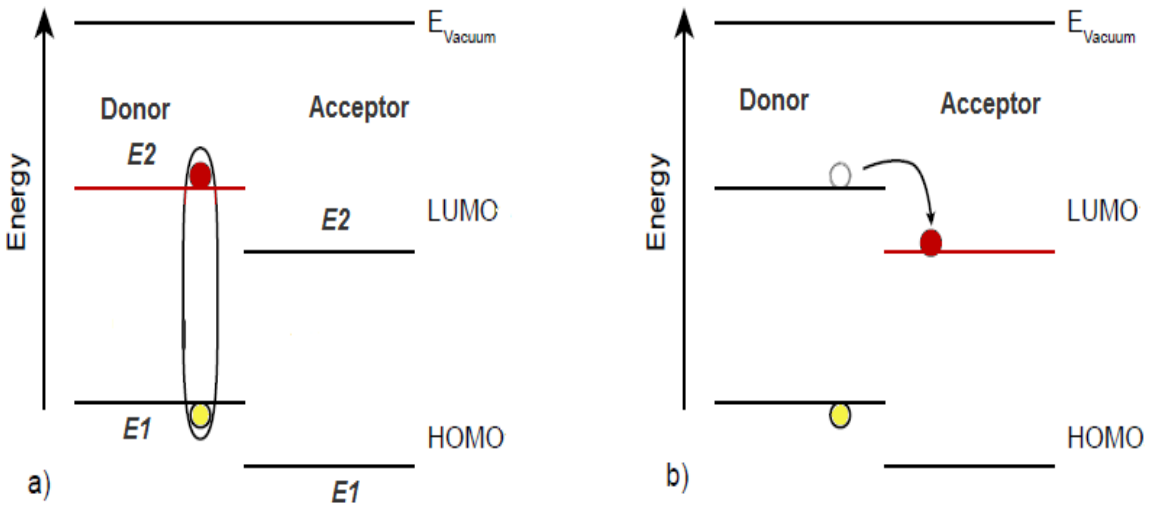

Figure 2.5: Energy Diagram of Charge Generation and Separation in Organic Solar Cells

2.2.2 Transportation of Charges

Upon the dissociation of excitons into free charge carriers, the charges have to move from the active layer to their respective electrode where they will be collected. The morphology of the active layer plays an important role in the charge carrier mobility, as well as the formation of percolation path [43]. The acceptor material has the tendency to form clusters or dendrites with length scales that often exceed the exciton diffusion length [15]. These length scales can be controlled by the concentrations of acceptor components in the active layers of P3HT: PCBM-based organic solar cells [16].

2.3 ARCHITECTURE OF ORGANIC SOLAR CELLS

The photoactive layer of organic solar cells is based on single, bi-layer and blend of two organic materials intimately mixed together. The efficiencies of organic solar cells depend on the robustness of the layered organic materials.

2.3.1 Single Layer Devices

This consists of a layer of polymer between two metal electrodes. In this structure, excitons can dissociate at only two interfaces. Low efficiencies are associated with single layer

solar cells due to poor electron mobilities [17].

2.3.2 Bilayer Devices

In bilayer devices, the p and n type materials are stacked up over each other, as shown in Figure 2.6. In these devices, only excitons produced within a distance of ~10-20 nm from the interface can reach the bulk heterojunction interface [18]. This leads to the loss of absorbed photons further away from the interface. It also results in devices with low quantum efficiencies. The efficiencies of bilayer solar cells are limited by the charge generation 10-20 nm around the donor-acceptor interface [44].

Thicker films induce optical filter effects in the absorbing material before the light reaches the interface. This results in a minimum photocurrent at the maximum of the optical absorption spectrum [19]. When the layer is too thick, the transit time of photo-generated charges becomes longer than the exciton lifetime. This leads to charge recombination. Hence, the thickness of the active layer must be controlled to avoid recombination of charges.

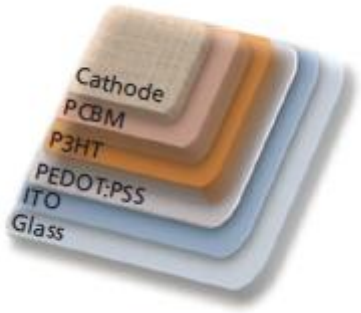

Figure 2.6: A Bilayer Organic Solar Cell

2.3.3 The Bulk Heterojunction Device.

This bulk heterojunction (BHJ) structure consists of a blend of polymers. The electron donating (p-type) material and the electron accepting (n-type) material are combined together in a film that is referred to as the active layer. Excitons created in the blend of donor-acceptor

material diffuse to the interface where charge separation takes place. Excitons generated in an organic solar cell usually have short diffusion lengths and low mobility. However, for efficient charge generation after the absorption of photons, each exciton created must reach an acceptor-donor interface within a short distance of a few nm, otherwise recombination will occur and such excitons will not contribute to charge generation [20]. In the case of BHJ solar cells, the active layers consist of mixtures of electron donors and acceptors that improve charge mobility. This reduces the extent of charge recombination, thereby increasing the overall device efficiencies.

However, a major problem with bulk heterojunction is that of solid-state miscibility. Yu et al. [20] have showed that the solvent used plays a key role, not only on the film quality, but also in determining the overall performance of the bulk heterojunction solar cell. Further work by Shaheen et al. [21] has also shown that the solid state morphology of the active layers in BHJ solar cells have important effects on their power conversion efficiencies. They achieved the first truly promising result for BHJ solar cells when mixing MDMO-PPV and PCBM in the ratio 1 to 4 by weight and optimizing nanoscale morphology of the film, yielding a power conversion efficiency of 2.5%.

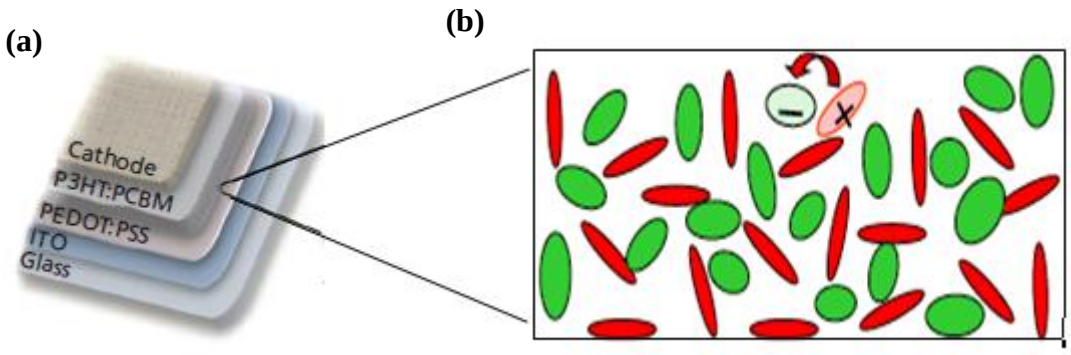

Figure 2.7: (a) A Bulk Heterojunction Solar Cells (b) Donor Acceptor Material

2.4 ACTIVE LAYER MATERIALS (ORGANIC MATERIALS)

2.4.1 Conjugated Polymers (Electron Donors)

Polymers are made up of long chain of repeating molecules. Conjugated polymers are polymers having alternating single and double bonds within their molecule. Conjugated polymers have electronic properties that resemble those of semi-conductors [48,50]. They also have the mechanical properties of polymers [48]. The first conducting polymer, polyacetylene, was discovered in 1977 [22].

A number of organic materials [Figures 2(a-i)] have been used as electron donors in organic photovoltaics. Polythiophenes and their derivatives such as Poly(3-alkylthiophene) (P3AT), poly(3-hexylthiophene) (P3HT). Thiophene rings are oriented in head to head (H-H), head to tail (H-T) and tail to tail (T-T). The HT–HT structure of polythiophenes is denoted as region-regular. While regioregularity is an important factor in characterization of polythiophenes, P3HT possesses a high regioregularity above 98%. This leads to high photovoltaic performance. Other polymers that are used as electron donors include: 2,1,3-benzothiadiazole based polymers (BT), Pyrrolo[3,4-c]pyrrole-1,4-dione (DPP) and derivatives, Benzo(1,2-b;4,5-b0)dithiophene-based polymers, etc.

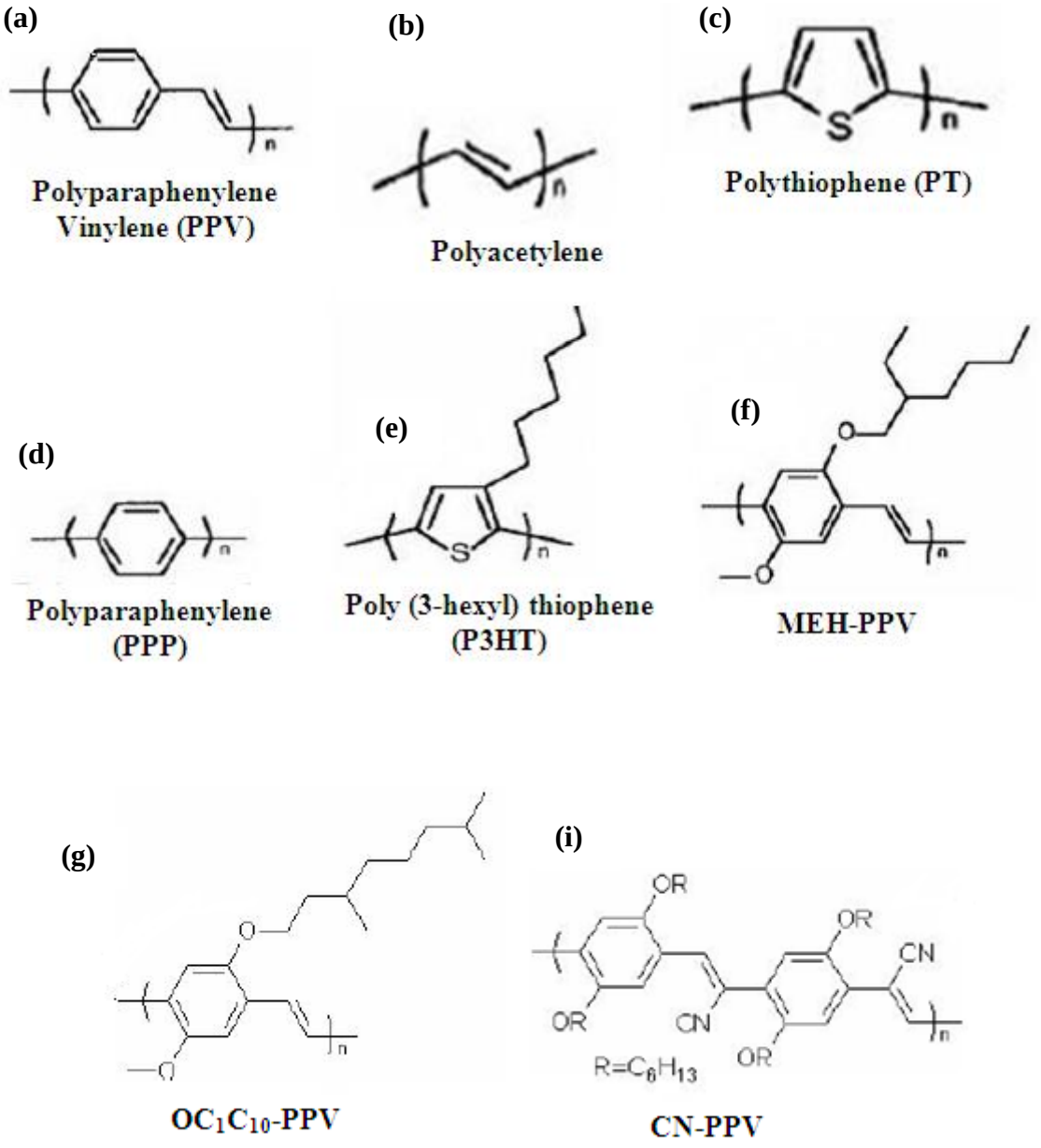

Figure 2.8: Molecular Structures of Some Organic Polymers

2.4.2 Electron Acceptors

For high efficient organic photovoltaic, electron acceptors consisting of fullerene and its derivatives have been the most successful due to their high electron mobility. $PC_{60}BM$ and its corresponding C_{70} derivative ($PC_{70}BM$) have been dominantly used as acceptors in organic photovoltaics fabrication.

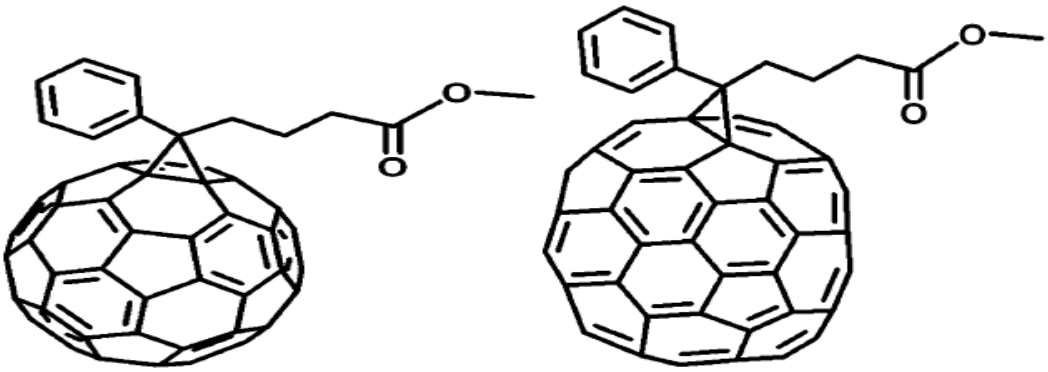

Figure 2.9: Fullerene Derivatives

2.5 SOLAR CELL CHARACTERIZATION

The performance and electrical characteristics of solar cell can be established by measuring the Current density-Voltage (J-V) characteristics both in dark and under illumination. The essential parameters that are generally worked with are; short circuit current density (*Jsc*), open circuit voltage (*Voc*), the fill factor (*FF*) and the power conversion efficiency (η). All these parameters can be deduced from the J-V curve of the solar cell.

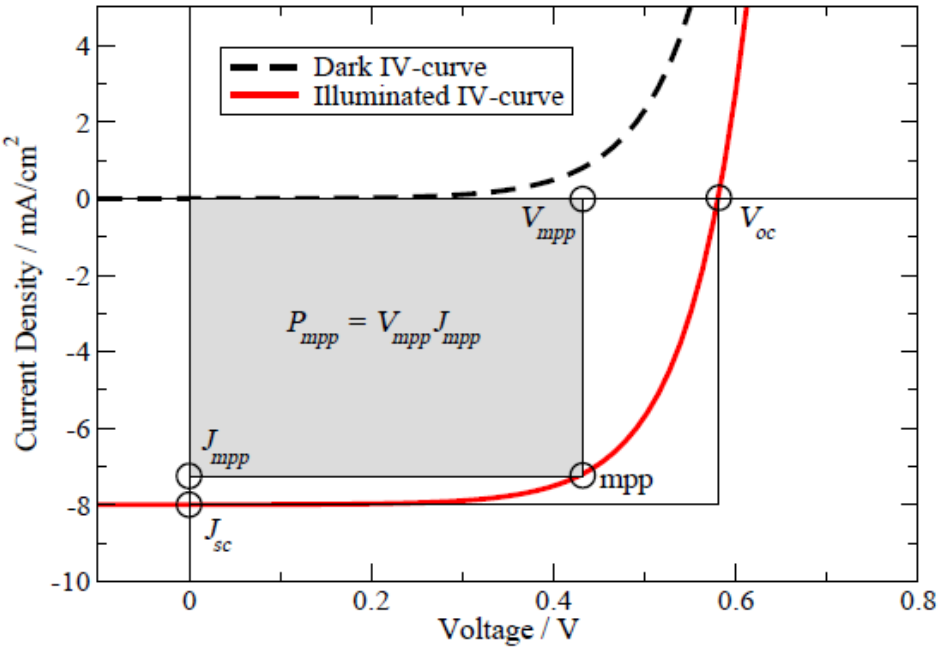

Figure 2.10: Typical Current Density-Voltage Characteristic of an Organic Solar Cell (Adapted from Ref. 3)

2.5.1 The Short Circuit Current Density (J_{sc})

This is the current density under illumination at zero applied bias. It is the current density when the applied voltage is zero. At this point, there is no power generated, but the J_{sc} marks the onset of power generation. In ideal devices, the J_{sc} is the same as the photocurrent density J_{ph}.

2.5.2 The Open Circuit Voltage (V_{oc})

The open-circuit voltage (V_{oc}) is the voltage across the solar cell, when the current density under illumination equals to zero. This is the same as the device being open-circuited. No power is actually produced at this voltage, since the current density is zero, and power is the product of current and voltage. This point also marks the boundary of power production in solar cells.

2.5.3 Fill factor (FF)

The fill factor relates the maximum power the cell can deliver, to the open circuit voltage and the short circuit current density. The maximum power produced (P_{max}) occurs at the voltage V_{max} and current-density J_{max} where the product of J and V is at a maximum in absolute value. The fill factor of a solar cell is defined as [52]:

$$FF = \frac{I_{max} V_{max}}{I_{sc} V_{oc}} \tag{2.2}$$

The fill factor is an indication of how close I_{max} and V_{max} come to the boundaries of power production of I_{sc} and V_{oc}. It is also an indication of the sharpness of the bend in the J-V curve that connects I_{sc} and V_{oc}.

2.5.4 Power conversion efficiency (η)

It is defined as the percentage of incident irradiance I_L (light power per unit area) that is converted into output power. Since the point where the cell operates on the I-V curve changes, depending on the load, the output power also depends on the load. The Power conversion efficiency is expressed as [52]:

$$\eta = \frac{|I_{max}|X\ V_{max}}{I_L} X100\% \quad = \quad \frac{FF\ X|I_{sc}|XV_{oc}}{I_L} X100\% \qquad (2.3)$$

The power conversion efficiency is important as it determines how effectively the space occupied by a solar cell is being used. It also determines how much area must be covered with solar cells to produce a given amount of power.

The power conversion efficiency relies greatly on the power and spectrum of the light source since solar cells do not absorb and convert photons to electrons at all wavelengths with the same efficiency. Even though the spectrum of the sunlight at the earth's surface varies with location, cloud coverage, and other factors, the air mass 1.5 spectrum (Figure 2.11) [23] is the most commonly used standard spectrum for measuring and comparing the performance of photovoltaics. Due to difficulties in recreating this exact spectrum in the laboratory with standard lamps, power conversion efficiency measurements must often be corrected based on the external quantum efficiency

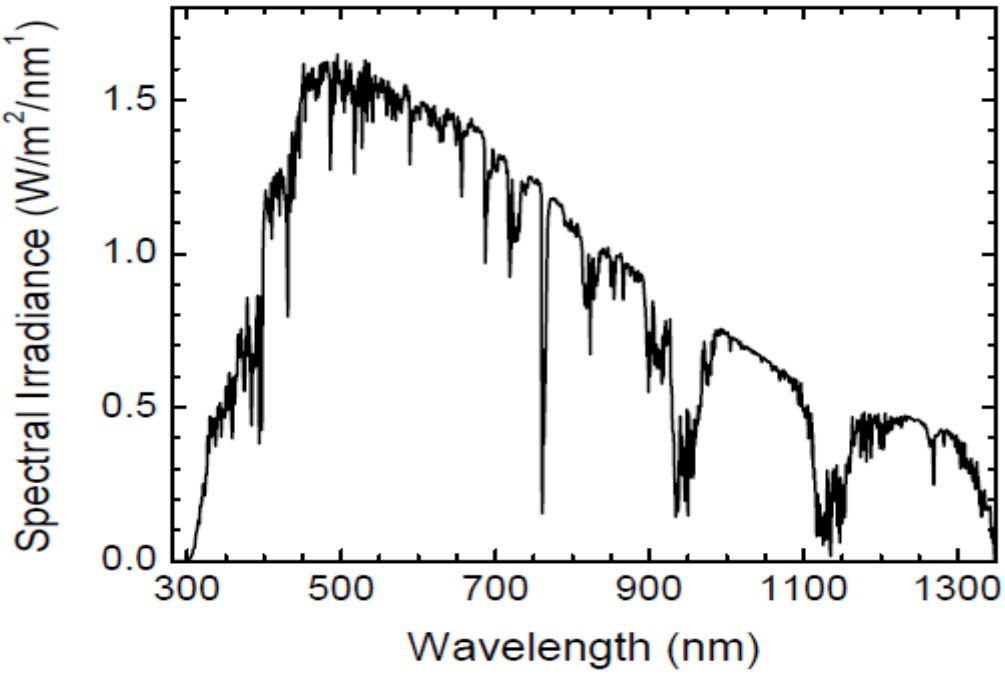

Figure 2.11: Spectral Irradiance of the AM1.5 G Solar Spectrum

2.5.5 External Quantum Efficiency (EQE)

The external quantum efficiency of a device is the fraction of incident photons converted into current. It depends on wavelength. This wavelength dependence is attributed to the correlation of absorption in the active layers with wavelength. The short-circuit current density expected under a light source can be estimated from the EQE and the spectral irradiance of the light source. This is achieved by integrating the product of the EQE and the photon flux density. For the standard AM1.5 G spectrum, the current density is expressed as:

$$J_{SC} = \int_0^{\infty} eEQE(\lambda)\frac{\lambda}{hc}E_{\lambda}^{AM1.5G}(\lambda)d\lambda \qquad (2.4)$$

where $E_{\lambda}^{AM1.5G}$ is the spectral irradiance of the AM1.5 G spectrum, λ is the wavelength, h is Planck's constant, *c* is the speed of light, and *e* is the elementary charge.

2.5 ACTIVE LAYER MORPHOLOGY

Significant work has been done to improve the morphology of the active layers of organic solar cells [43,52]. Several methods have been explored to achieve better performance of solar cells [21,22,38]. In organic solar cells, it has been found that the morphology of the active layer has a very important impact on the device efficiency [24-27]. This results in remarkable differences within one material system, just by varying the preparation conditions. Several studies have been carried out to determine the relation between the morphology and efficiency of organic solar cells [43]. A wide range of morphologies have also been produced by varying the preparation conditions and techniques [24,32,41].

This control of morphology is the most complicated and most investigated part of organic solar cell fabrication. A number of preparation conditions like solvents used to dissolve donor-acceptor materials, donor-acceptor ratios, annealing effects and additives are required to induce the correct morphology. At large polymer domain sizes, excitons will be lost due to exciton decay or recombination.

A range of morphology imaging tools including scanning electron microscopy (SEM),

transmission electron microscopy (TEM), selected area electron diffraction (SAED), scanning probe microscopy (SPM) and atomic force microscopy (AFM), can be used for the characterization of the active layer morphology [28].

2.6.1 Effects of Donor-Acceptor Mixing Ratios

The effect of the mixing ratio of a donor-acceptor heterojunction on the formation, dissociation and recombination of charge-transfer excitons was studied by Veldman et al. [29]. They used atomic force microscopy (AFM) and transmission electron microscopy (TEM) on blend films with a broad range of mixing ratios. They found that, at low concentrations, the PCBM is finely dispersed in the polymer. In contrast, at very high concentrations, the PCBM tends to aggregate to form crystalline domains with sizes of about 100 nm. Simultaneously, they performed time-resolved photoluminescence measurements and found that the emission from the charge-transfer exciton, which decayed within a few nanoseconds in the near infrared wavelength region, is dependent on this variation in morphology. They also found that the lifetime of the emission is reduced at higher PCBM concentrations. This implies that the charge-transfer excitons are depopulated much faster, provided that the recombination to the ground state is not accelerated by the addition of PCBM. This suggests that the charge-transfer excitons are separated into free charge carriers more efficiently if the phase segregation between the polymer and the PCBM phases is increased.

2.6.2 Effect of Solvent on Morphology of Blends of Active Materials

Quist et al. [30] performed time-dependent microwave photoconductivity experiments and TEM on blends of MDMO-PPV and PCBM. Their studies were carried out on a range of compositions using chlorobenzene and toluene, respectively, as organic solvents [31]. They observed phase segregation and the formation of nanocrystallites at higher concentrations of PCBM. Interestingly, they found that the amount of the segregation was different for the two solvents used, with stronger segregation being observed in toluene cast films.

2.6.3 Effects of Annealing on Morphology of Blends of Active Materials

The morphology of the active layer can be modified through thermal and solvent annealing [4,53]. Zhao et al [45] have showed that annealing of P3HT at temperatures higher than its glass transition leads to improved crystallinity. Post-production thermal annealing is often done at temperatures up to 150^0C [46]. Kim et al [32] carried out an extensive study in which they varied annealing temperatures and solvent choice. They found that more efficient cells were produced by annealing at 140^0C for the P3HT: PCBM of ratio 1:1 BHJ system. Similar studies [33] also show the effects of thermal annealing of an optimally loaded P3HT: PCBM blend (1:0.8 weight ratio), where annealing treatment at 155^0C gave comparable results. P3HT: PCBM films gives rise to P3HT crystallites when annealed, where P3HT main chains orient parallel, and their side chains perpendicular, to the substrate.

During annealing, the structure of the active layer, which has been frozen when the solvent evaporated during spin-coating, can relax to an energetically more favourable configuration. Annealing helps to increase the size of the donor-acceptor domains in the blend. This increases the distance excitons need to travel to dissociate at the heterojunction interface. Recent studies [34] shows that charge separation is slower in annealed P3HT: PCBM blends as a result of the increased domain size. The increase in domain size equally enhances charge carrier mobility and, therefore, the recombination mechanisms in the device [35].

2.6.4 Effects of Crystallinity on the Efficiency of Bulk Heterojunction Solar Cells

In a recent study by Michael L et al, [54] thermal annealing has been shown to increase the total population and ordering of P3HT crystallites. In their study, they used a combination of grazing incidence wide angle X-ray scattering and Current-Voltage characteristics of the solar cells produced to investigate the effects of morphology on photo conversion efficiency. They observed that the increase in the population of crystallites formed at a short annealing time of 5minutes leads to an increase in J_{sc}, fill factor and improved photo conversion efficiency. The increase in the total

population of P3HT crystallite in the blend ultimately leads to increase in light absorption and charge carrier mobility. At annealing temperatures below 170^0C, the molecular ordering of PCBM is not obvious, but upon increase in temperature to 180^0C, PCBM crystallites were seen which they believed will serve to form percolation pathway for better efficient cells. However, higher annealing temperatures lead to formation of micron scale crystals of PCBM. The presence of large PCBM crystals makes charge hopping in the blend more difficult thereby reducing photo conversion efficiency.

In another study by Akogwu et al, [24] thermal annealing at critical temperatures resulted in formation of fractal dendritic patterns on the P3HT/PCBM blend leading to poor electrical properties of the devices. The dendrite formed in the blend was believed to have hampered efficient exciton dissociation, as a good interface between donor and acceptor component is required for efficient charge separation. They observed that the dendritic growth emanated from PCBM, Further growth of the crystals deplete the polymer matrix which is required for effective nanoscale charge hopping. Thus, lower power conversion efficiency is recorded for devices with such growths.

2.7 Deposition Techniques Involved in the Fabrication of Organic Solar Cells

Several techniques have been used for the deposition of layers in organic solar cells. Some of these techniques include: magnetron sputtering for the deposition of the anodic transparent conducting oxide; spin-coating for the deposition photoactive polymers and hole-injection layers, and thermal evaporation for the deposition of metal electrodes.

2.7.1 Magnetron Sputtering Deposition

Sputtering occurs whenever any particle strikes a surface with enough energy to dislodge an atom from the surface. Sputtering can be induced by means of plasmas that generate charged particles that are electrically accelerated towards a surface. Sputtering deposition is done in two modes namely: direct current (DC) and radio frequency modes. RF sputtering is a technique that is

used to create thin films, such as those found in the computer and semiconductor industry. Like direct current (DC) sputtering, RF sputtering involves running an energetic wave through an inert gas to create positive ions. The target material, which will ultimately become the thin film coating, is struck by these ions and broken up into a fine spray that covers the substrate, the inner base of the thin film.

RF sputtering differs from DC sputtering in the voltage, system pressure, sputter deposition pattern, and ideal type of target material. During an RF sputtering process, the target material, substrate, and RF electrodes begin in a vacuum chamber. Next, the inert gas, which is usually argon, neon, or krypton, depending on the size of the target material's molecules, is directed into the chamber. The RF power source is then turned on, sending radio waves through the plasma to ionize the gas atoms. Once the ions begin to contact the target material, they are fragmented is broken into small pieces that travel to the substrate and begin to form a coating. The incident particle impacts the surface or near-surface atoms of the solid with sufficient energy to break bonds and dislodge atoms. If, during this process, one or more atoms are removed from the solid, they are considered to be sputtered atoms. A schematic illustration of RF sputtering is presented below in Figure 2.12.

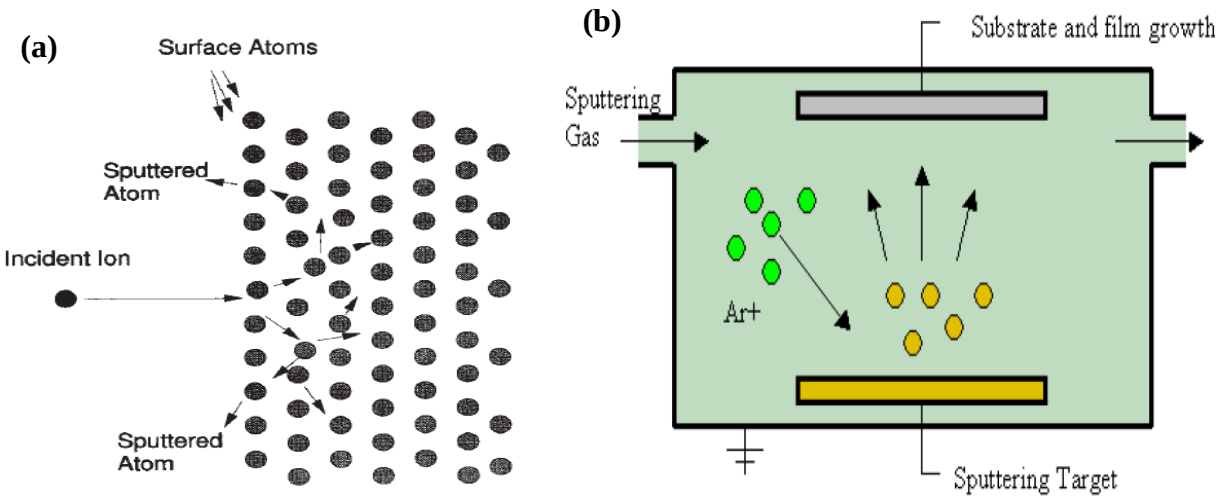

Figure 2.12: Schematic of the Sputtering System

2.7.2 Spin-Coating Techniques

Spin Coating involves the acceleration of a liquid puddle on a rotating substrate. The coating material is deposited in the center of the substrate, either manually, or by a robotic arm. Spin coating is the most common technique for the deposition of organic polymers in preparation of organic solar cells. This technique is cheaper and easier to use, compared to most deposition techniques. It allows for uniform deposition onto flat substrates. The following basic stages (Figure 2.13) are involved in the spin coating technique:

1. The polymer is dispensed onto the substrate;
2. The polymer is spread across the substrate (by spinning at approximately 500 rpm), and
3. The substrate is then spun at a higher speed (2000-4000 rpm) and allowed to dry.

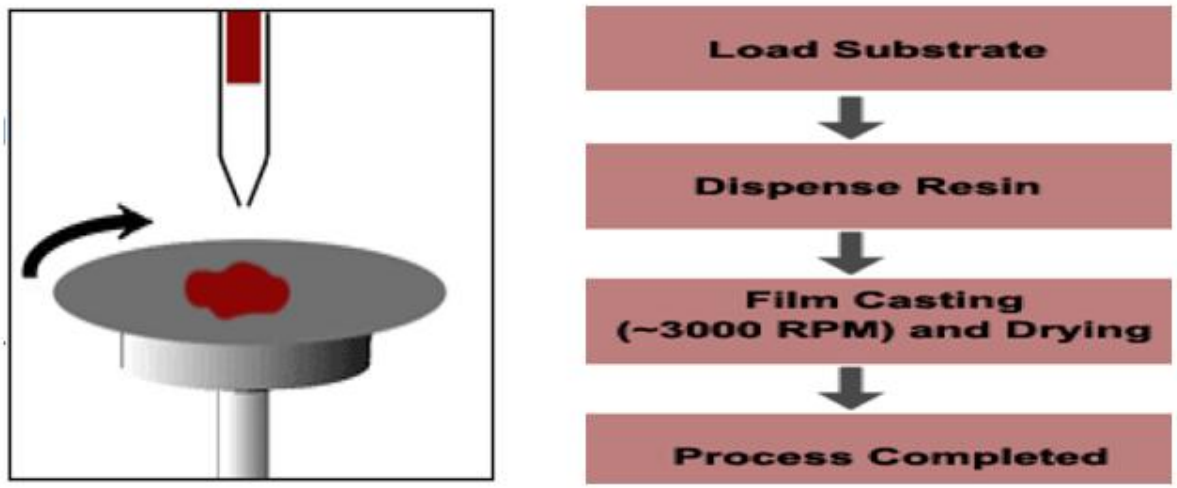

Figure 2.13: The Spin-Coating Process

There are two common methods of dispensing. They include: static dispensing and dynamic dispensing. Static dispensing involves depositing a small puddle of fluid on or near the center of the substrate. The volume of the puddle depends on the viscosity of the fluid and the size of the substrate to be coated. Higher viscosity and or larger substrates typically require larger puddles to ensure full coverage of the substrate during the high speed spin step. Dynamic dispensing is the

process of dispensing, while the substrate is turning at low speed. A speed of about 500 rpm is commonly used during this step of the process. This serves to spread the fluid over the substrate and can result in less waste of resin material, since it is usually not necessary to deposit as much to wet the entire surface of the substrate. This is an attractive method when the fluid or substrate itself has poor wetting characteristics. It can also eliminate voids that may otherwise form.

2.7.3 Thermal Evaporation of Cathode Layer

Thermal Evaporation is a deposition technique that is used for coating many types of materials in a highly evacuated chamber. The material to be deposited is usually heated to its vaporized state by a high voltage applied as heat energy to a heating filament. The filament heats up the metal, which is then irradiated in straight lines onto the substrate that is placed directly above it under high vacuum. The melting temperature of the heating filament or coil is greater than that of material to be deposited.

The Thermal Vacuum Evaporation technique is most suitable for deposition of highly-reactive cathode materials, such as aluminum and calcium. The method is clean and allows a improved contact between the layer of deposited material and the surface upon which it has been deposited. Since evaporated beams travel in straight lines at very high vacuum, precise and uniform patterns are produced. A schematic of the thermal evaporation process (in vacuum) is shown below in Figure 2.14.

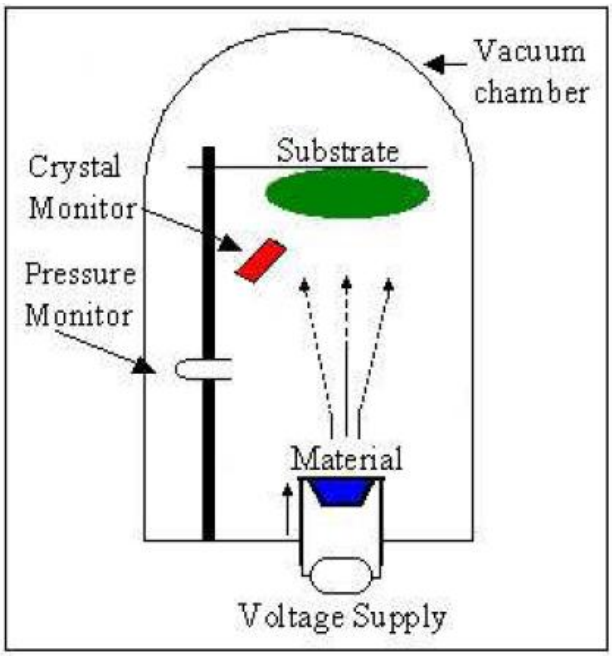

Figure 2.14: Schematic of thermal evaporation in vacuum

2.9 REFERENCES

[1] Ifor D. W. Samuel and Graham A. Turnbull, Materials today, September 2004 (pages 28-35)

[2] Fullerene based Organic Solar Cells; Lacramioara Mihaela Popescu

[3] Identification and Analysis of Key Parameters in Organic Solar Cells, Moritz K. Riede

[4] Ji HyeJeon , HangKenLee, DongHwanWanga, JongHyeokPark , OOkPark ;"The role of non-solvent swelling in bulk hetero junction solar cells", *Solar Energy Materials & Solar Cells 102 (2012) 196–200*

[5] H. Shirakawa, A. G. MacDiarmid, A. J. Heeger, *Chem. Commun.* **2003**, 1.

[6] H. Shirakawa, *Angew. Chem. Int. Ed.* **2001**, *40*, 2574.

[7] A. G. MacDiarmid, *Angew. Chem. Int. Ed.* **2001**, *40*, 2581.

[8] A. J. Heeger, *Angew. Chem. Int. Ed.* **2001**, *40*, 2591.

[9] R. H. Friend, R. W. Gymer, A. B. Holmes, J. H. Burroughes, R. N. Marks, C. Taliani, D. D. C. Bradley, D.A. Dos Santos, J.L. Brédas, M. Löglund, W.R. Salaneck, *Nature* **1999**, *397*, 121.

[10] J. H. Burroughes, D. D. C. Bradley, A. R. Brown, R. N. Marks, K. Mackay, R. H. Friend, P. L. Burns, A. B. Holmes, *Nature* **1990**, *347*, 539.

[11] *Tom J. Savenije*

[12] Exciton Recombination In The Fullerene Phase Of Bulk Heterojunction Organic Solar Cells; George Frederick Burkhard April 2011

[13] Ashcroft, N. W. & Mermin, N. D. *Solid State Physics*. (Holt, Reinhart, and Winston, 1976).

[14] C. J. Brabec, V. Dyakonov, J. Parisi, and N. S. Sariciftci. Organic Photovoltaics Concepts and Realization. Springer, Berlin, 1 edition, 2003.

[15] H. Hoppe, M. Niggemann, C. Winder, J. Kraut, R. Hiesgen, A. Hinsch, D. Meissner, and N. S. Sariciftci. Nanoscale morphology of conjugated polymer/fullerene-based bulk heterojunction solar cells. Advanced Functional Materials, 14(10):10051011, 2004.

[16] W. L. Ma, C. Y. Yang, X. Gong, K. Lee, and A. J. Heeger. Thermally stable, efficient polymer solar cells with nanoscale control of the interpenetrating network morphology. Advanced Functional Materials,

[17] R. N. Marks, J. J. M. Halls, D. D. C. Bradley, R. H. Friend, and A. B. Holmes. The photovoltaic response in poly (phenylene-vinylene) thin- film devices. Journal of Physics-Condensed Matter, 6(7):1379–1394, 1994.

[18] Winder, C.; Sariciftci, N. S. *J. Mater. Chem*. **2004**, *14*, 1077.

[19] Harrison, M. G.; Gruener, J.; Spencer, G. C. W. *Phys. Re*v. *B* **1997**, *55*, 7831.

[20] G. Yu, J. Gao, J. C. Hummelen, F. Wudl, A. J. Heeger, *Polymer photovoltaic cells enhanced efficiencies via a network of internal donor-acceptor heterojunctions,* Science 270 (1995), 1789.

[21] S. E. Shaheen, C. J. Brabec, N. S. Sariciftci, F. Padinger, T. Fromherz, J. C. Hummelen, *2.5% efficient organic plastic solar cells*, Applied Physics Letters **78** (2001), 841.

[22] C.K. Chiang, C.R. Fincher, Y.W. Park, A.J. Heeger, H. Shirawaka, E.J. Louis, S.C. Gau, and A.G. MacDiarmid. Electrical conductivity in doped polyacetylene. Physical Review Letters, 39(17):1098 – 1101, 1977.

[23] IEC-904-3, IEC Standard

[24] Onobu Akogwu, Wali Akande, Tiffany Tong, and Wole Soboyejo; "Dendrite growth in annealed polymer blends for use in bulk heterojunction solar cells" *J. Appl. Phys.* ***110****, 103517 (2011)*

[25] F. Padinger, R. S. Rittberger, and N. S. Sariciftci. Effects of postproduction treatment on plastic solar cells. Advanced Functional Materials, 13(1):85–88, January 2003.

[26] H. Hoppe, T. Glatzel, M. Niggemann, W. Schwinger, F. Schaeffler, A. Hinsch, M. C. Lux-Steiner, and N. S. Sariciftci. Efficiency limiting morphological factors of MDMO-PPV:PCBM plastic solar cells. Thin Solid Films, 511:587–592, July 2006.

[27] G. Li, V. Shrotriya, Y. Yao, J. S. Huang, and Y. Yang. Manipulating regioregular poly(3-hexylthiophene): [6,6]-phenyl-c-61-butyric acid methyl ester blends – route towards high efficiency polymer solar cells. Journal Of Materials Chemistry, 17(30):3126–3140, 2007.

[28] X Yang, J Loos, *Macromolecules* **2007**, 40, 1353-1362.

[29] Veldman, D.; Ipek, O.; Meskers, S. C. J.; Sweelssen, J.; Koetse, M. M.; Veenstra, S. C.;

Kroon, J. M.; Bavel, S. S. v.; Loos, J.; Janssen, R. A. J. *Journal of the American Chemical Society* **2008**, *130*, 7721.

[30] Quist, P. A. C.; Martens, T.; Manca, J. V.; Savenije, T. J.; Siebbeles, L. D. A. *Solar Energy Materials and Solar Cells* **2006**, *90*, 362.

[31] Zhang, F.; Jespersen, K. G.; Björström, C.; Svensson, M.; Andersson, M. R.; Sundström, V.; Magnusson, K.; Moons, E.; Yartsev, A.; Inganäs, O. *Advanced Functional Materials* **2006**, *16*, 667.

[32] Kim Y, Choulis SA, Nelson J *et al*. (2005) Device annealing effect in organic solar cells with blends of regioregular poly (3-hexylthiophene) and soluble fullerene. *Applied Physics Letters* **86**: 063502–063503.

[33] Reyes-Reyes M, Kim K and Carroll DL (2005) High efficiency photovoltaic devices based on annealed poly (3-hexylthiophene) and 1-(3-methoxycarbonyl)-propyl-1- phenyl-(6, 6) C blends. *Applied Physics Letters* **87**: 083506.

[34] R. A. Marsh, J. M. Hodgkiss, S. Albert-Seifried, R. H. Friend, *Nano Lett.* **2010**, *10*, 923.

[35] Li, G. *et al.* "Solvent Annealing" Effect in Polymer Solar Cells Based on Poly(3-hexylthiophene) and Methanofullerenes. *Adv. Funct. Mater.* **17**, 1636-1644 (2007).

[36] Jianhui Hou, Mi-Hyae Park, Shaoqing Zhang, Yan Yao, Li-Min Chen, Juo-Hao Li, and Yang Yang, *Macromolecules* **2008**, *41*, 6012-6018

[37] Stephen R. Forrest, Nature Vol. 428 (29 April 2004)

[38] J. M. J. Frechet and B. C. Thompson, Angew. Chem. Int. Ed. 2008, 47, 58–77

[39] Gustav Edman Jonsson, Hans Fredriksson, Raja Sellappan and Dinko Chakarov, International Journal of photoenergy, Vol 2011, Article ID 939807.

[40] Yuanzuo Li, Tonu Pullerits, Meiyu Zhao and Mengtao Sun, pubs.acs.org/JPCC

[41] Travis L. Benanti & D. Venkataraman;" Organic solar cells: An overview focusing on active layer morphology", *Springer -Photosynthesis Research (2006) 87: 73–81*

[42] Qingxin Yang, Matthias Muntwiler, and X.-Y. Zhu, PHYSICAL REVIEW B **80**, 115214 (2009)

[43] D Chirvase1, J Parisi1, J C Hummelen2 and V Dyakonov, Nanotechnology 15 (2004) 1317–1323

[44] Serap Gunes, Helmut Neugebauer, and Niyazi Serdar Sariciftci, Chem. Rev. **2007,** 107, 1324-1338

[45] Zhao, J. et al. (2009). Phase Diagram of P3HT PCBM Blends and Its Implication for the Stability of Morphology. *Journal of Physical Chemistry B*, 113(6), 1587-1591.

[46] Shinuk Cho and Kwanghee Lee, JOURNAL OF APPLIED PHYSICS **100**, 114503 (2006)

[47] P. Peumans, A. Yakimov, and S. R. Forrest, "Small molecular weight organic thin-film

photodetectors and solar cells," J. Appl. Phys., vol. 93, pp. 3693–3723, 2003.

[48] H. Hoppe and N. S. Sariciftci, "Organic solar cells: An overview," J. Mater. Res, vol. 19, pp. 1924-1945, 2004.

[49] K. M. Coakley and M. D. McGehee, "Conjugated polymer photovoltaic cells," Chem. Mater., vol. 16, pp. 4533–4542, 2004.

[50] Weder, C., Ed.; P*oly(arylene ethynylene)s - From Synthesis to Applications*; Advances in Polymer Science Series Vol. 177; Springer, Heidelberg, **2005**

[51] Gang Li, Vishal Shrotriya, Yan Yao, and Yang Yang, "Investigation of annealing effects and film thickness dependenceof polymer solar cells based on poly 3-hexylthiophene", Journal of Applied Physics 98, 043704 (2005)

[52] Mikkel Jorgensen, Kion Norrman, Frederik C. Krebs, "Stability/degradation of polymer solar cells", *Solar Energy Materials & Solar Cells 92 (2008) 686–714*

[53] Tetsuro Hori, Varutt Kittichungchit, Hiroki Moritou, Hitoshi Kubo, Akihiko Fujii and Masanori Ozaki, "Solvent Vapor Treatment Effects on Poly(3-hexylthiophene) Thin Films and its Application for Interpenetrating Heterojunction Organic Solar Cells" *Materials 2010, 3, 4939-4949*

[54] Neil D. Treat, Chris G. Shuttle, Michael F. Toney, Craig J. Hawker and Michael L. Chabinyc; "In situ measurement of power conversion efficiency and molecular ordering during thermal annealing in P3HT:PCBM bulk heterojunction solar cells", *J. Mater. Chem., 2011, 21, 15224*

CHAPTER 3

EXPERIMENTAL PROCEDURES

3.1 Instruments/ Materials Used

The following instruments and materials were used for this experimental work:

- RF sputtering machine with ITO target
- Thermal Evaporator
- Spin Coater
- Scanning Electron Microscope
- Veeco Dektak 150 Film Surface Profiler
- Keithley Source Meter
- UV/VIS Spectrophotometer
- Ultrasonic bath
- Magnetic Stirrer
- Digital Multimeter
- Hot plate
- Furnace
- Beakers
- Tweezers
- Regio-regular poly(3-hexylthiophene-2,5-diyl) (P3HT)
- [6,6]-phenyl-C61-butyric acid methyl ester (PCBM)
- Poly(3,4-ethylenedioxythiophene) (PEDOT) doped by the organic acid poly(styrene-sulfonate) (PSS) (PEDOT: PSS)
- Chlorobenzene (Organic Solvent)
- Decon-90

- Acetone
- Ethanol
- De-ionized water
- Isopropyl alcohol (IPA)

3.2 Fabrication of Organic Solar Cells

The fabrication of the solar cells was carried out in the following order: cleaning of glass slides; sputtering of ITO on glass slides; spin-coating of an hole injection layer (PEDOT:PSS); spin-coating of the active layer (P3HT:PCBM); thermal annealing of the active layer and finally, thermal evaporation of the top cathode (Aluminum).

3.2.1 Cleaning of Glass Slides

The cleaning of the glass slides was done in a fume hood. First, the glass slides were cut into 2.5 cm x 2.5 cm (approx.1sq inch) squares with a glass cutter before washing carefully with decon-90 for 10 minutes. The glass slides were then rinsed 10 times in distilled water and 5 times in ethanol. They were then soaked in acetone for about 5 minutes and further remove any organic substance from the glass slides by placing them in an ultrasonic bath for 10 minutes at 25^0C. The samples were removed from the ultrasonic bath, rinsed with ethanol and immediately blow-dried using Nitrogen gas.

3.2.2. Deposition and Annealing of Indium Tin-Oxide

Indium Tin-Oxide was sputtered unto clean glass slides with an Edwards R.F. Magnetron sputtering system (Edwards Auto 306, Edwards, Sanborn, NY, USA) operated at an initial vacuum pressure of $2.9 \times 10^{-5}\ Torr$ and an R.F. power of 50 W. The sputtering was carried out at room-temperature $(27^oC - 32^oC)$. Argon was introduced to excite ions on the ITO target. The initial deposition rate was $0.12\ \dot{A/s}$. An ITO film thickness of 100 nm was achieved at this deposition rate after one hour. This was achieved with an average deposition rate of $0.8\ \dot{A/s}$ and a pressure of

$3.0 \times 10^{-3} Torr$. Figure 3.1 shows the set- up that was used for the sputtering process. The ITO-coated glass was then annealed at $250^{o}C$ for $1h$ to change the ITO layer from armorphous to crystalline phase.

3.2.3 Spin-Coating of PEDOT:PSS

PEDOT: PSS is purchased from H. C. Starck (Newton, MA). This was used as the hole extraction material. The solution of PEDOT:PSS was filtered through a 0.25 μm mesh size filter paper. This was done to ensure a smooth layer when spin-coated. The PEDOT: PSS was spin-coated for 60 seconds at a speed of 1500 revolution per minute (rpm) using a Laurell Spin coater (Laurell WS650HZ-23NPP/A3/AR2, Laurell Technologies, North Wales, Pennsylvania, USA). By smearing the glass surface with several drops of polymer solution in a static dispense mode, a 100nm thick of PEDOT:PSS was spin-coated on all the ITO-coated glasses. The samples were further dried in an oven for 5 minutes before confirming the thickness using a surface profiler. The set-up of the spin coating process is shown below in Figure 3.1

Figure 3.1: Spin Coating Set-up

3.2.4 Spin-Coating Annealing of P3HT: PCBM

The active layer is made up of a blend of donor and acceptor components namely poly(3-hexylthiophene) (P3HT) and [6,6]-phenyl C61-butyric acid methylester (PCBM). P3HT and PCBM solutes were dissolved in chlorobenzene with a ratio of 1:0.8 by weight. The mixture was placed on KIKA Larbortechnik Digital Magnetic stirrer and allowed to stir continuously for 6 hours at a speed of 500 rpm. The beaker used for stirring was completely covered from a ray of light using an aluminum foil, as exposure to light could cause degradation of the active components.

The solution of P3HT: PCBM was filtered into a beaker using $0.25\mu m$, mesh before mounting the PEDOT: PSS/ITO/glass on the stub of a spin coater. A 100 nm thick P3HT: PCBM was spin coated on the samples at a speed 2000 rpm for 60 seconds. The thickness was also confirmed using surface profiler. The samples of the deposited P3HT:PCBM on PEDOT:PSS/ITO-coated glass were annealed for 10 min at different temperatures: $50^oC, 100^oC,\ 150^oC,\ 200^oC$ and room temperature.

3.2.5 Thermal Evaporation of Aluminum Cathode

A 99.99% pure Al rod was dropped in tungsten evaporating boat. The samples were then loaded in the chamber of an Edwards 306 thermal vacuum evaporator (Edwards Auto 306, Edwards, Sanborn, NY, USA) (Figure 3.2). The chamber was closed and a liquid Nitrogen gas was poured to the system for achieving a high vacuum pressure of $2.5 \times 10^{-5}\ Torr$. Once sufficient vacuum of $2.5 \times 10^{-5}\ Torr$ is reached, the evaporation was started. At an average deposition pressure of $3 \times 10^{-3}\ Torr$, a 150nm thick Al was thermally deposited on P3HT:PCBM/PEDOT:PSS/ITO/ glass samples. The thickness was also checked by using surface profiler.

Figure 3.2: Edwards Auto 306 Thermal Vacuum Evaporator

3.3 CHARACTERIZATION OF ORGANIC SOLAR CELLS

The behavior of the bulk heterojunction structures produced was characterized to determine their optical properties, morphology and electrical properties.

3.3.1 Morphology of the P3HT:PCBM

The morphologies of the annealed P3HT:PCBM were observed using a Scanning Electron Microscope (SEM) and an optical microscope. The surface roughness of the deposited layers of organic solar cells was measured by moving the stylus of a profiler vertically to contact with the layer and then laterally moved it across it for a distance of $2000\ \mu m$. The annealed samples were viewed under a Carl Zeiss Scanning Electron Microscope (EVO MA 10, Carl Zeiss

SMT, Oberkochen, Germany) .This was used to observe the changes in microstructure in each of the active layers. The samples were attached to aluminum stubs using double sided conductive tape that were fixed to the sample holder. This is then mounted on the stage of the SEM. An acceleration voltage of 5keV was supplied to the filament, while the detector was set to secondary electron imaging (SEI) mode.

3.3.2 Optical Measurements

The optical transmittance and reflectance were measured using a UV/VIS AVASPEC 128 Fibre-Optic Spectrophotometer (Avantes BV, USA). For the transmittance, air was used as a control to ensure 100% transmittance before mounting the sample gently on a sample holder between the light source and light detector before turning on the switch. The optical transmittance of the annealed and unannealed P3HT:PCBM layer was measured. Similarly, a perfectly reflective silicon wafer was used as a control for the maximum reflectance of light. This was checked before using the sample to measure optical reflectance. The laboratory set-up for the optical measurement is shown below in Figure 3.3

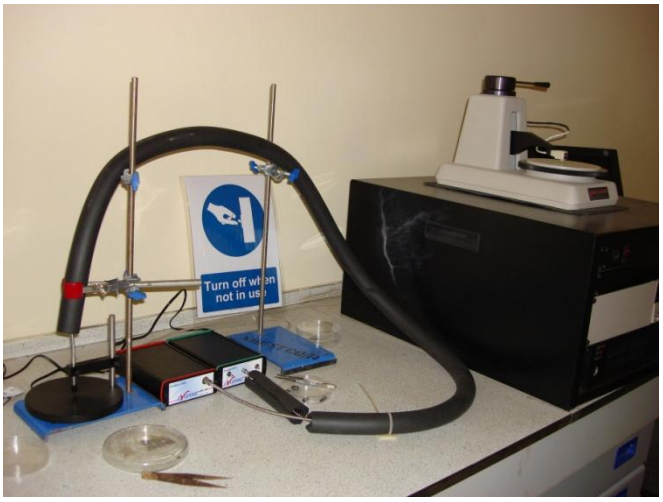

Figure 3.3: AVASPEC Fiber Optic Spectrophotometer

3.3.3 Electrical Characterization of OPV

For the organic solar cells, a clip was used to fix the position of the fabricated device. The two terminals of the wires from Keithley 2400SMU (Keithley instruments, Cleveland, Ohio, USA) (Figure 3.4) were connected to the electrodes of the device (one terminal was connected to the front anodic ITO while the other one was connected to the cathodic aluminium). A multimeter was used to check continuity of the connections. The instruments were switched on and voltage was sourced from 0 to 0.7 V with a step size of 0.05 V on the Labtracer software, before running the test to measure and save the I-V curves of all the devices at different annealing temperatures. Moreover, the sheet resistance of the annealed P3HT:PCBM layers was measured using the Keithley 2400 SMU set-up.

Figure 3.4: Keithley Source Meter Unit Set-up

CHAPTER FOUR

RESULTS AND DISCUSSIONS

4.1 MORPHOLOGY OF THE ACTIVE LAYER

The observed optical micrographs of the P3HT:PCBM active layers annealed at different temperatures are shown in Figure 4.1(a-e). The sample annealed at 50^0C shows a number of equiaxed PCBM crystals in the matrix of P3HT. These crystals are more evident and more abundant at annealing temperature of 150^0C where the grains transform from equiaxed particles and begin to assume needle like patterns. It is noted that the crystals formed are larger and denser. The images obtained from the blend annealed at 150^0C suggest that the needle like crystals formed is due to the fast diffusion of PCBM in the P3HT and result in extreme phase segregation. The same trend in the morphology (as shown in Figure 4.2 (a-d)) of the active layers subjected to the same annealing conditions was observed under Atomic Force Microscope (AFM) using tapping mode.

Figure 4.5 is the result showing the effect of annealing temperature on the grain size of crystals that are formed. Increasing annealing temperature increases the grain size of the P3HT:PCBM. The grain size starts decreasing from annealing temperature 150^oC upon further increase in temperature. Dendritic features were observed in P3HT:PCBM of ratio 1:1 (Figure 4.3b), while the features seemed clustered as the concentration of PCBM increases in the blend of P3HT:PCBM (as shown in Figures 4.3(c, d)).

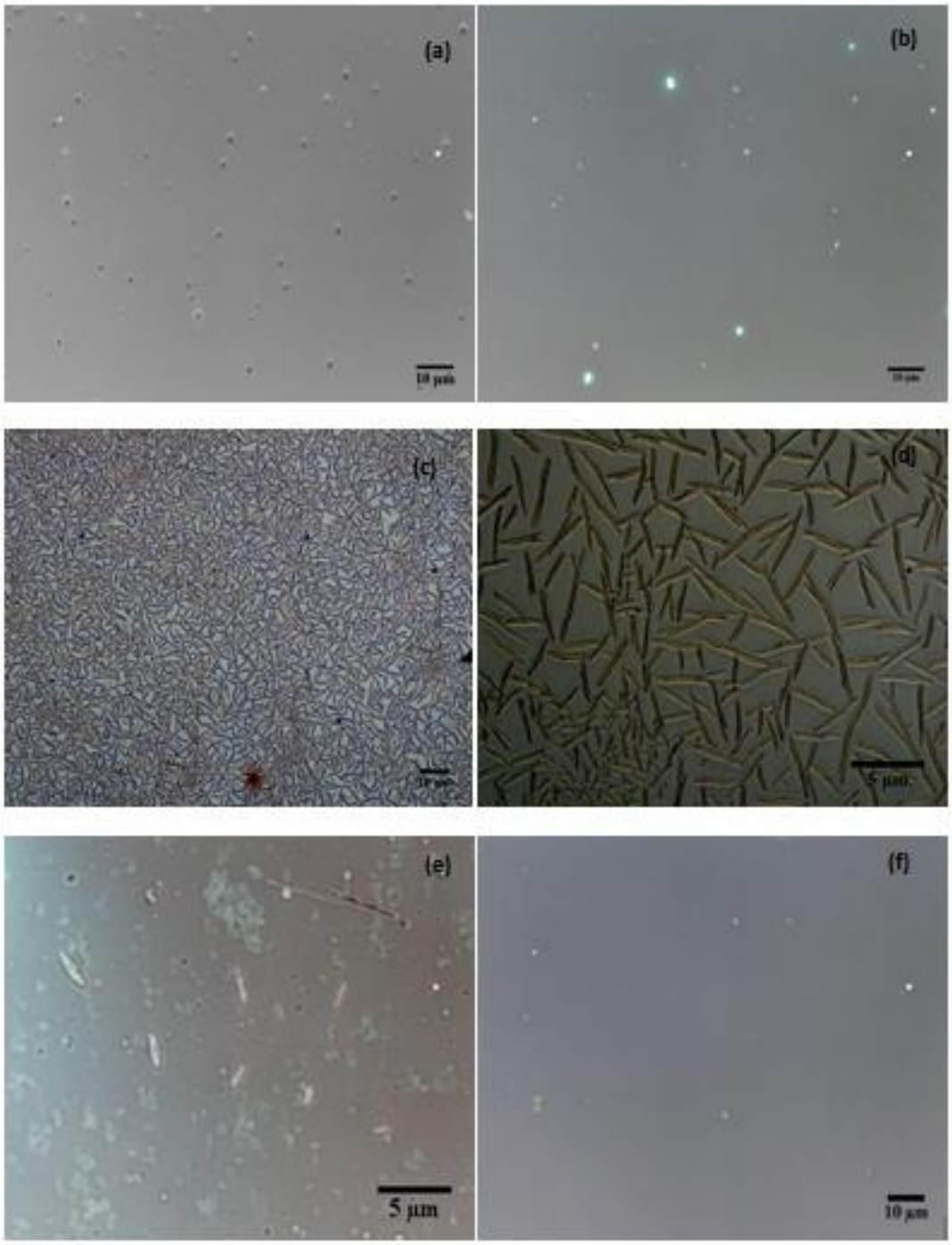

(e)

Figure 4.1: Optical images of active layers annealed at (a) 50^0C (b) 100^0C (c &d) 150^0C (e) 200^0C (f) RT

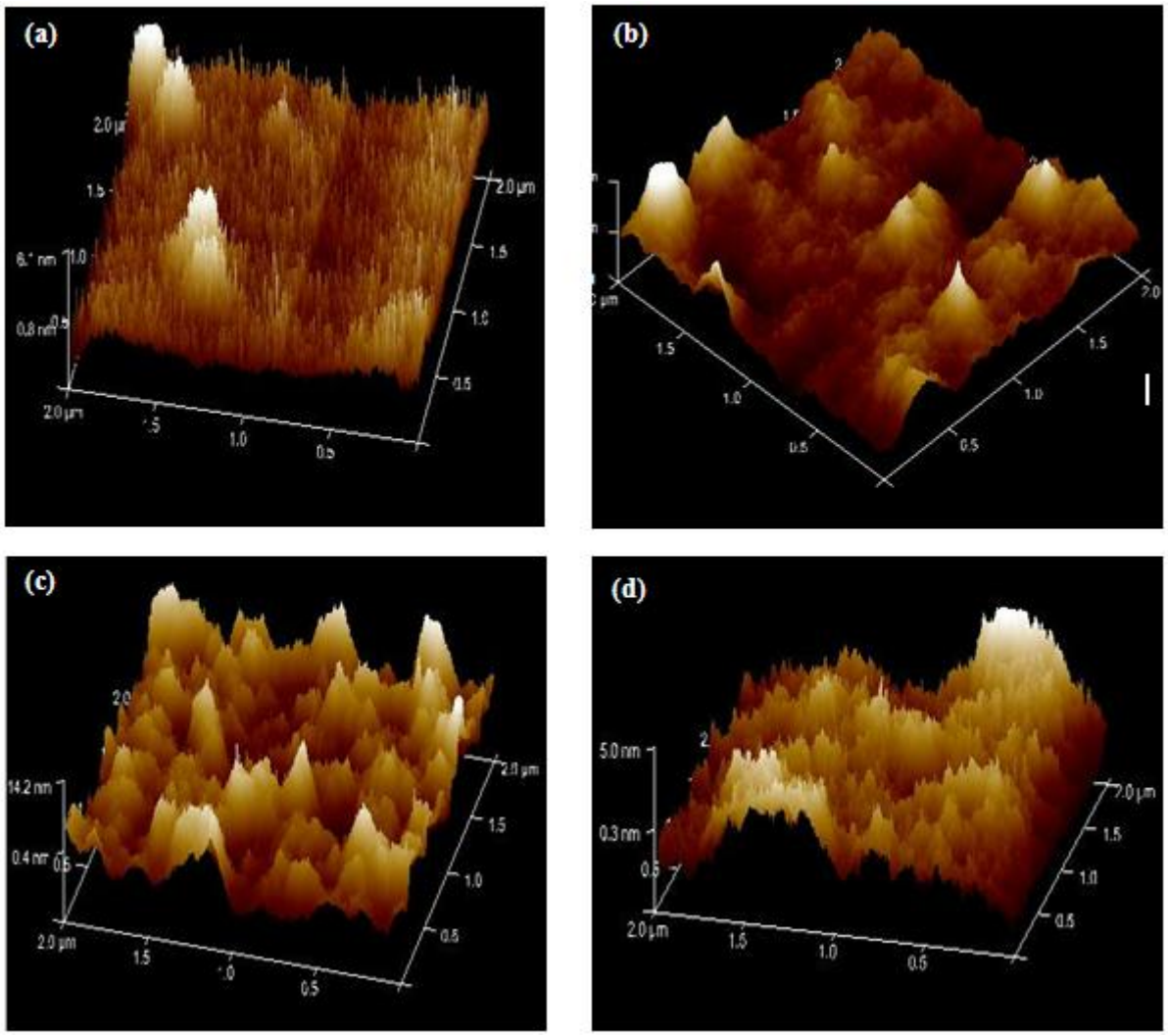

Figure 4.2: AFM Images of Active Layers Annealed at (a) 50^0C (b) 100^0C (c) 150^0C (d) 200^0C

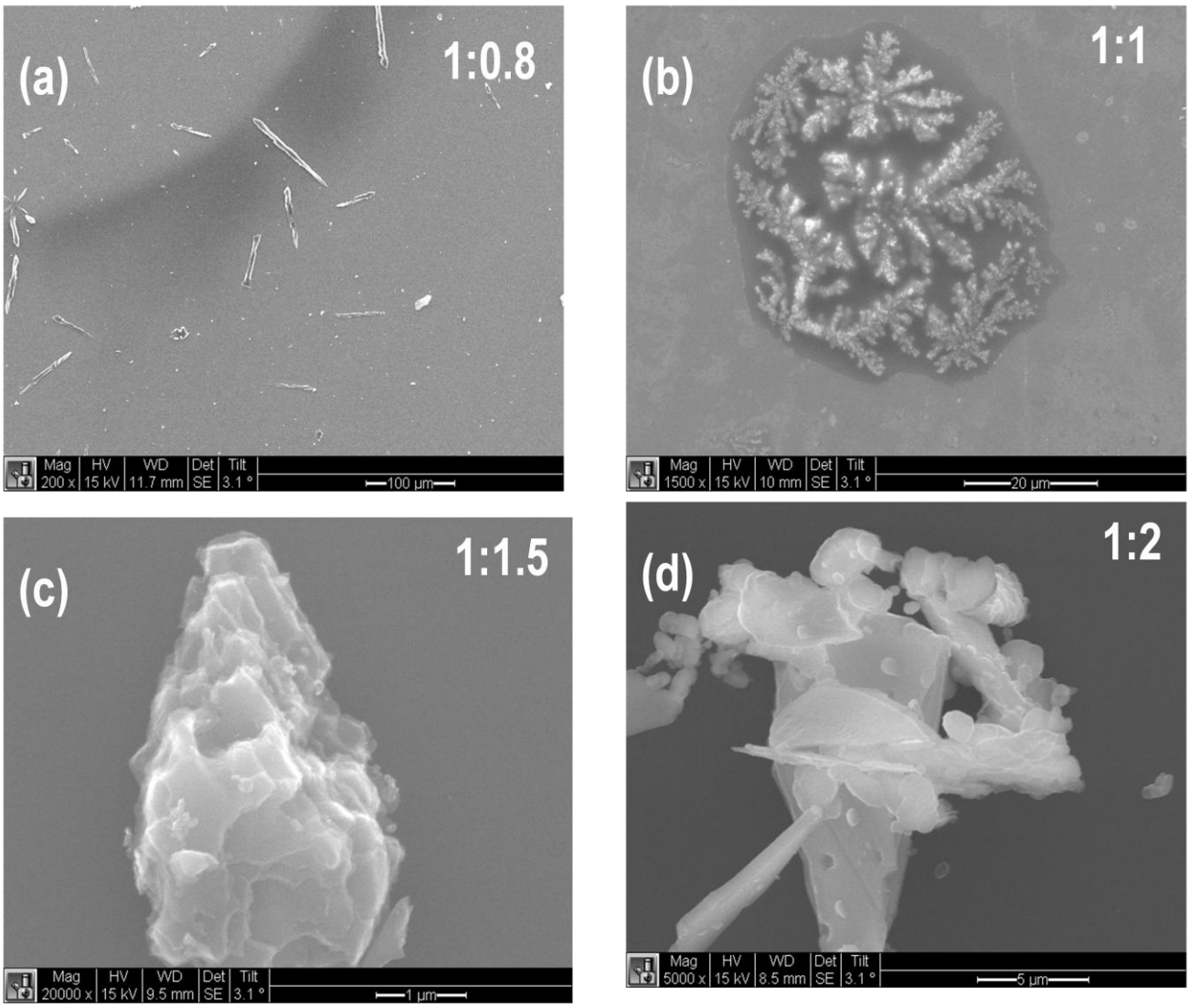

Figure 4.3: SEM images of P3HT:PCBM blend for different mixing ratios

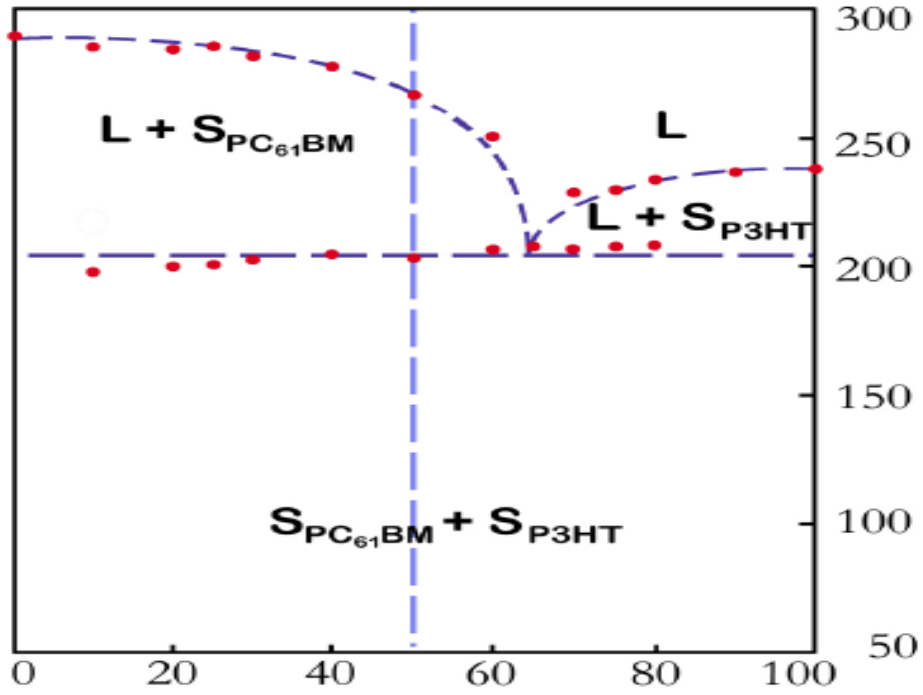

Figure 4.4: An *Eutectic Phase Diagram of P3HT:PCBM Adapted from* Ref. *[2]*

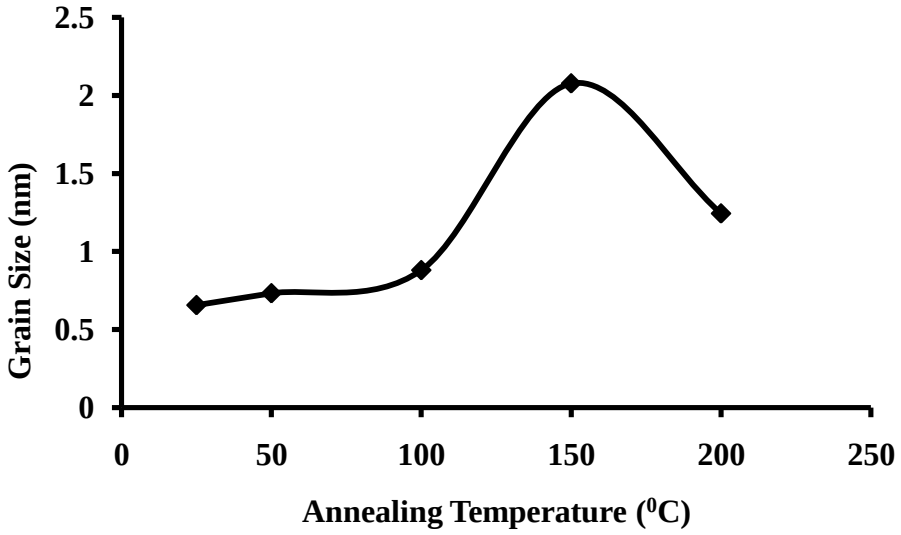

Figure 4.5: A Graph of Grain Size of the Active Layers as a Function of Annealing Temperatures

4.2 OPTICAL PROPERTIES OF ACTIVE LAYERS

The measured optical absorbance of the annealed and unannealed (Room Temperature) active layers is presented in figure 4.6. During annealing of the active layers, a colour change was observed as the film gets darker in colour and this gives an indication that there is a change in the

optical property of the film. Figure 4.6 shows that there is a modification in the absorption spectrum of P3HT:PCBM as the annealed layers shows an hyperchromic behaviour where there is an increase in the absorptivity with increase in annealing temperature. The peak was presented at a wavelength of about 500nm which is the absorption wavelength of P3HT [1]. This result establishes that the optical absorbance of P3HT:PCBM film is improved by thermal annealing. Moreover, the observed increase in absorbance shows that there is polymer ordering in P3HT as a result of thermal treatment.

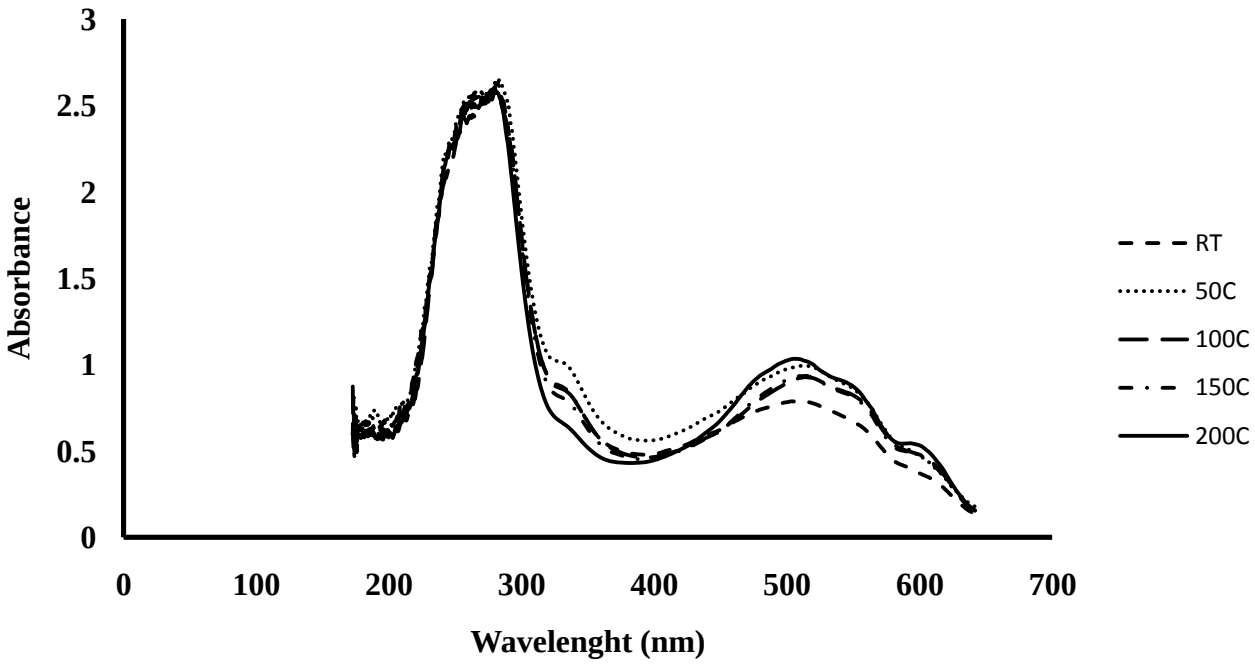

Figure 4.6: The Optical Absorbance of P3HT:PCBM at Different Annealing Temperatures

4.2.1 Effects of Annealing Temperature on Grain Size and Optical Properties

The estimated grain size of the blend of P3HT:PCBM increases as the annealing temperature increases to 150^{o}C but reduces upon further increase in the annealing temperature. This indicates that high annealing temperature could damage the blend of P3HT:PCBM-based bulk heterojunction solar cells. Similarly, the measured optical transmittance of the P3HT:PCBM increases with increase in annealing temperature. A high absorbance at the annealing temperature 50^{o}Ccould be attributed to error due to vibration.

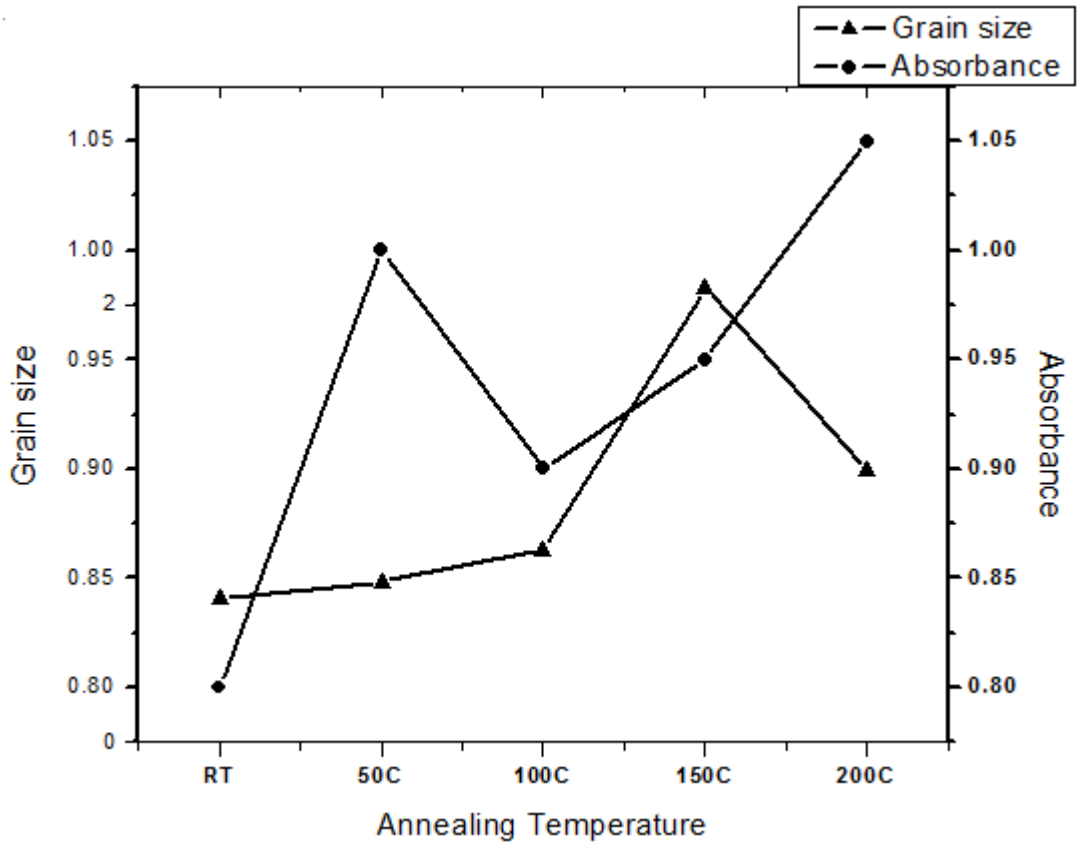

Figure 4.7: Graphs of Grain Size and Absorbance of the Active Layers as a Function of Annealing Temperatures

4.3 ELECTRICAL PROPERTIES OF THE BULK HETEROJUNCTION SOLAR CELLS

4.3.1 Current-Voltage (I-V) Curves at Different Annealing Temperatures

The current-voltage curves and the power-voltage of the devices fabricated at different annealing temperatures of the blend of P3HT:PCBM are shown in Figures 4.8(a-e) and 4.9(a-e) respectively. Values obtained from the main parameters such as the open circuit voltage (V_{oc}), short circuit current (I_{sc}), maximum power (P_{max}). The values were used to estimate the fill factor (FF) of the devices using equation (2.2). The summary of results is presented in table 4.1. From the result, devices made from annealed at 200^{o}C and the unannealed blend of P3HT:PCBM have lowest fill factor. Increasing annealing temperature increases the carrier mobility. However, the gradual reduction in the fill factor of the devices prepared from the active layer annealed at 150^{0}C and 200^{0}C can be attributed to severe phase segregation thus leading to higher recombination losses.

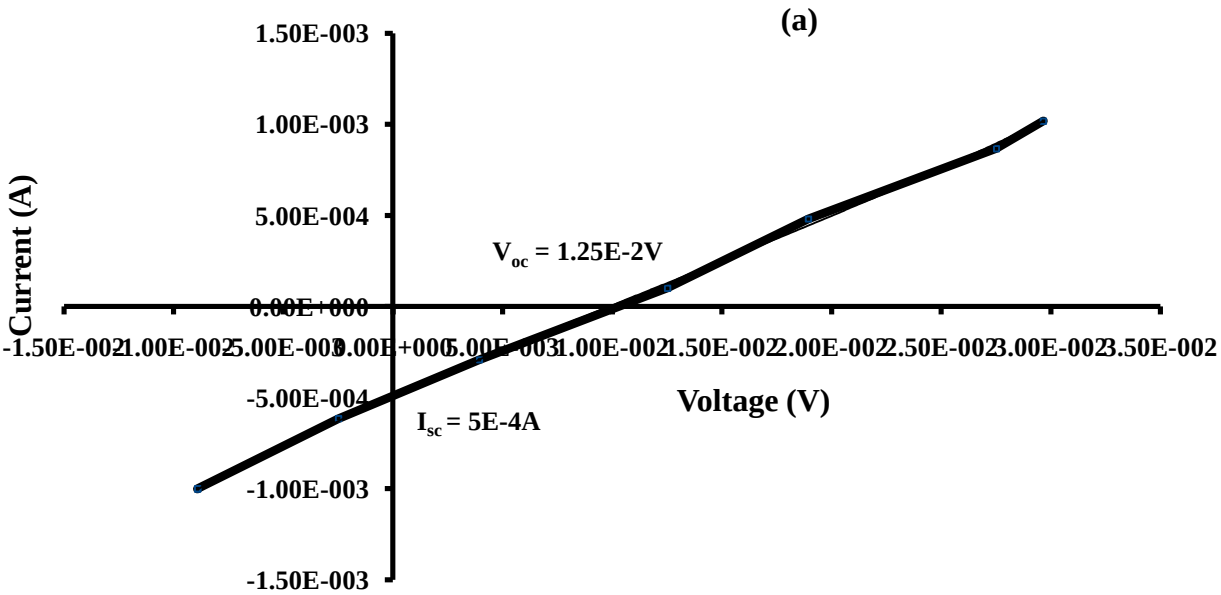
(a)
1.50E-003
1.00E-003
5.00E-004
0.00E+000
-5.00E-004
-1.00E-003
-1.50E-003
Current (A)
V_{oc} = 1.25E-2V
I_{sc} = 5E-4A
Voltage (V)

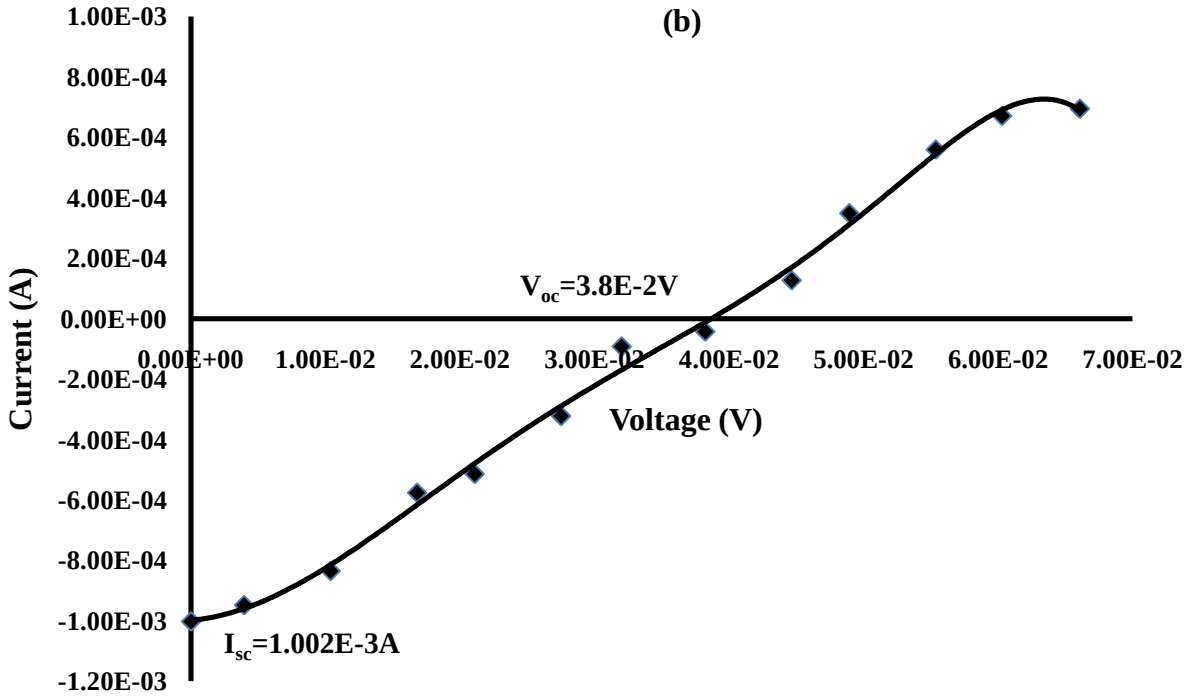
(b)
1.00E-03
8.00E-04
6.00E-04
4.00E-04
2.00E-04
0.00E+00
-2.00E-04
-4.00E-04
-6.00E-04
-8.00E-04
-1.00E-03
-1.20E-03
Current (A)
V_{oc}=3.8E-2V
I_{sc}=1.002E-3A
0.00E+00
1.00E-02
2.00E-02
3.00E-02
4.00E-02
5.00E-02
6.00E-02
7.00E-02
Voltage (V)

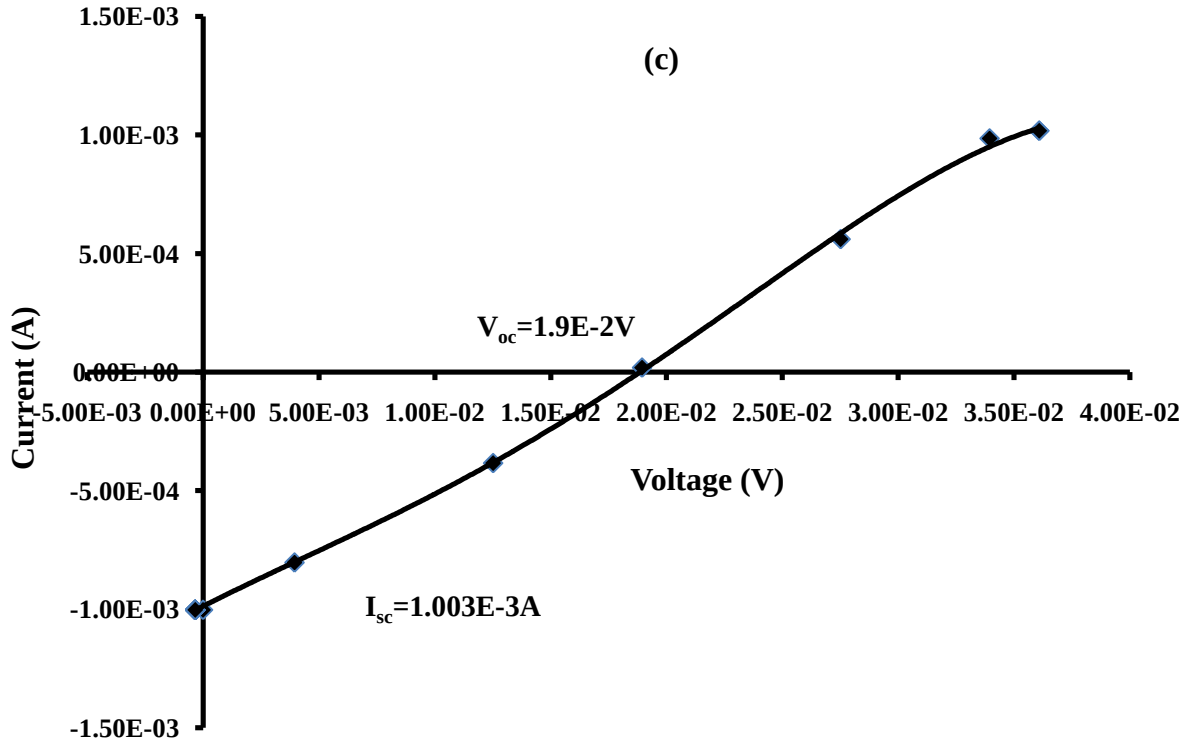
(c)
1.50E-03
1.00E-03
5.00E-04
0.00E+00
-5.00E-04
-1.00E-03
-1.50E-03
-5.00E-03 0.00E+00 5.00E-03 1.00E-02 1.50E-02 2.00E-02 2.50E-02 3.00E-02 3.50E-02 4.00E-02
Current (A)
Voltage (V)
V_{oc}=1.9E-2V
I_{sc}=1.003E-3A

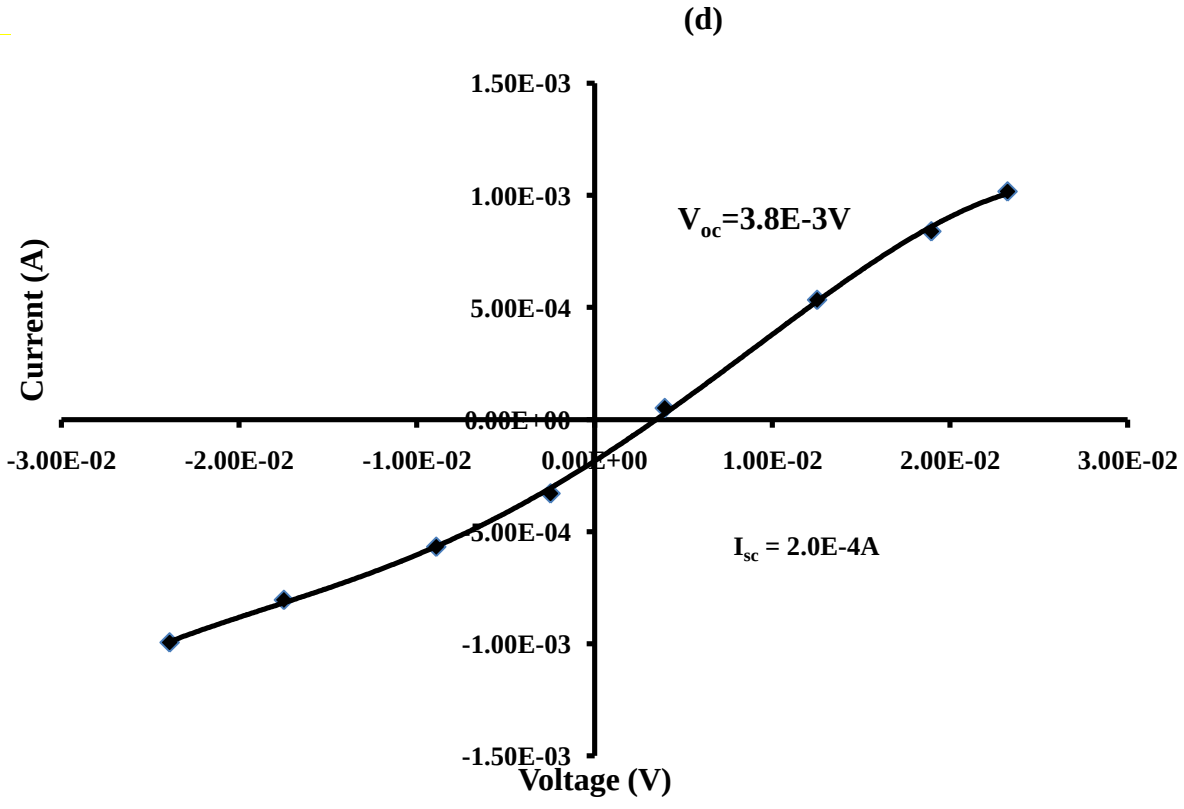
(d)
1.50E-03
1.00E-03
5.00E-04
0.00E+00
-5.00E-04
-1.00E-03
-1.50E-03
-3.00E-02 -2.00E-02 -1.00E-02 0.00E+00 1.00E-02 2.00E-02 3.00E-02
Current (A)
Voltage (V)
V_{oc}=3.8E-3V
I_{sc} = 2.0E-4A

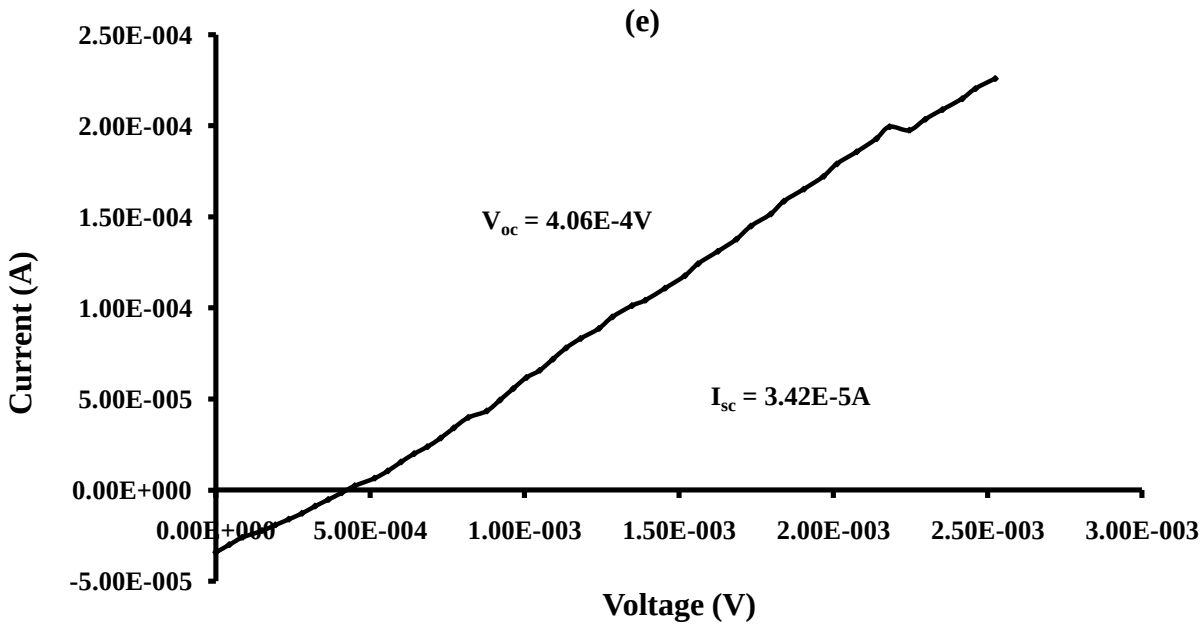

Figure 4.8: I-V Curves of the Devices Made from Active Layer Annealed at: (a) RT (b) 50^{o}C (c) 100^{o}C (d) 150^{o}C (e) 200^{o}C

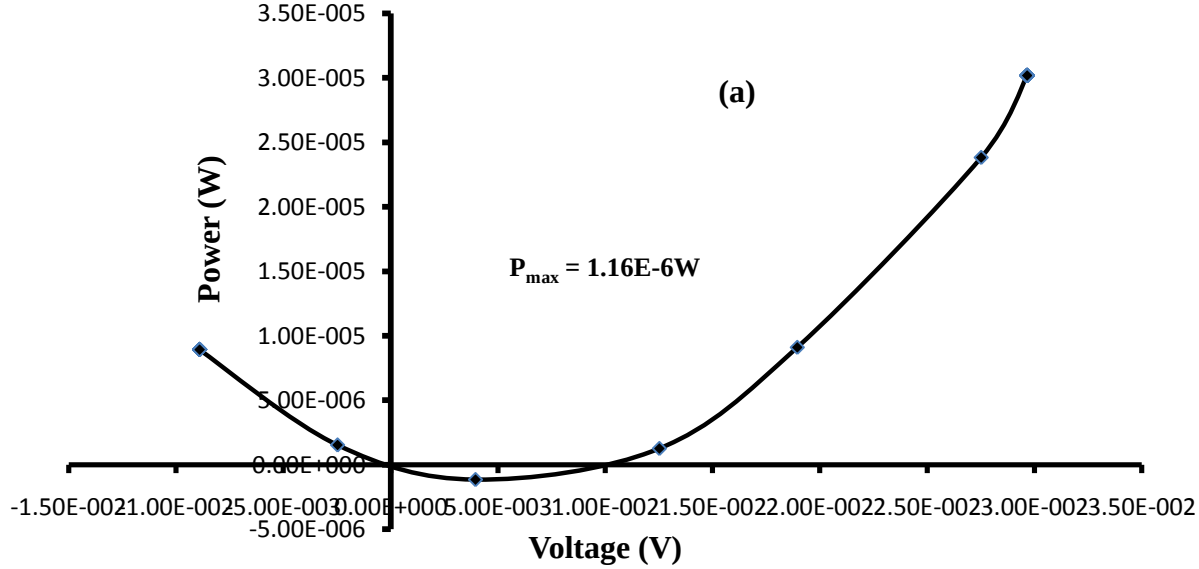
(a)
Power (W)
Voltage (V)
P_{max} = 1.16E-6W
3.50E-005
3.00E-005
2.50E-005
2.00E-005
1.50E-005
1.00E-005
5.00E-006
0.00E+000
-5.00E-006
-1.50E-002
1.00E-002
5.00E-003
0.00E+000
5.00E-003
1.00E-002
1.50E-002
2.00E-002
2.50E-002
3.00E-002
3.50E-002

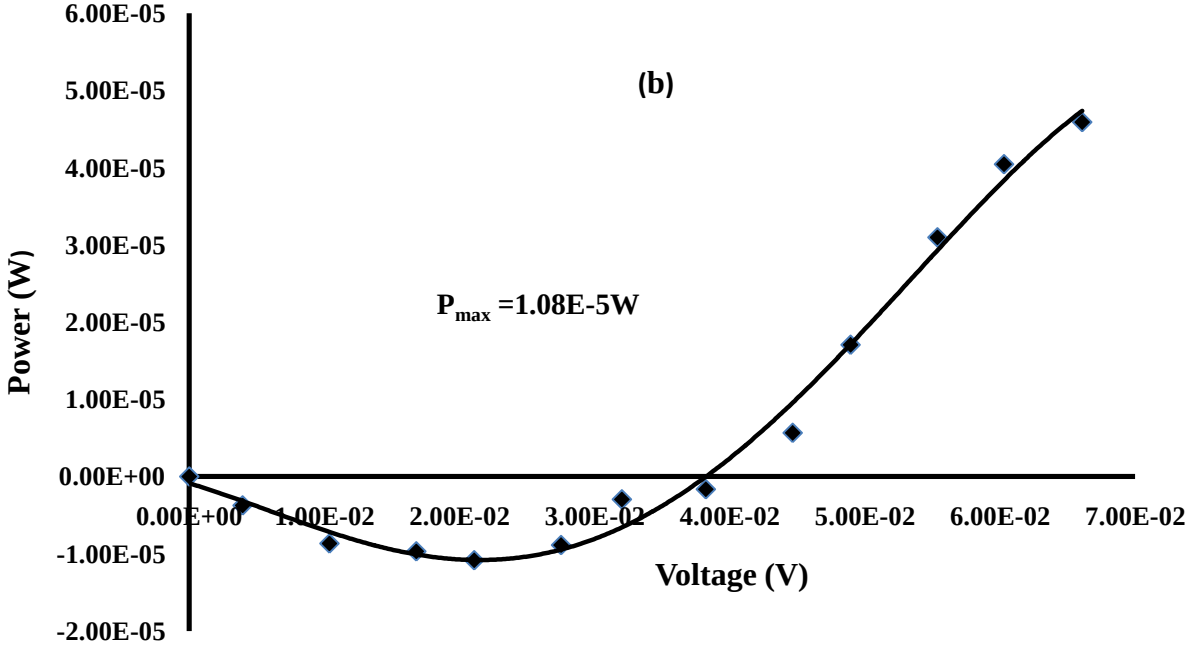
(b)
Power (W)
Voltage (V)
P_{max} =1.08E-5W
6.00E-05
5.00E-05
4.00E-05
3.00E-05
2.00E-05
1.00E-05
0.00E+00
-1.00E-05
-2.00E-05
0.00E+00
1.00E-02
2.00E-02
3.00E-02
4.00E-02
5.00E-02
6.00E-02
7.00E-02

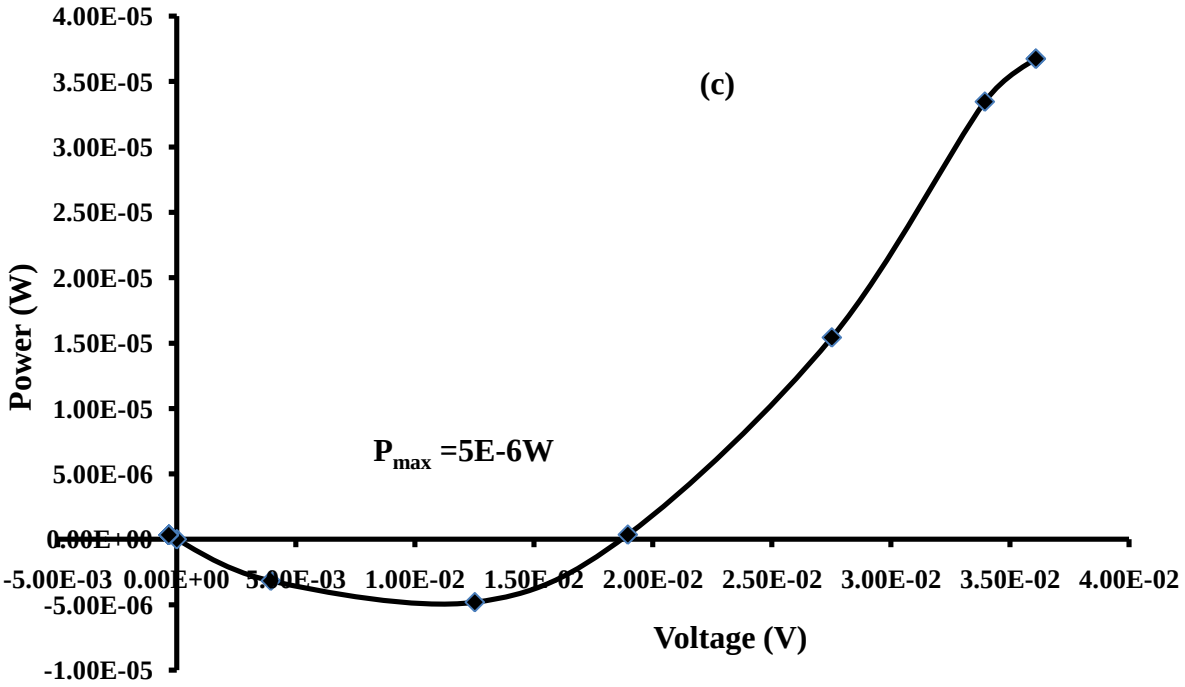
(c)
Power (W)
4.00E-05
3.50E-05
3.00E-05
2.50E-05
2.00E-05
1.50E-05
1.00E-05
5.00E-06
0.00E+00
-5.00E-06
-1.00E-05
P_{max} =5E-6W
-5.00E-03
0.00E+00
5.00E-03
1.00E-02
1.50E-02
2.00E-02
2.50E-02
3.00E-02
3.50E-02
4.00E-02
Voltage (V)

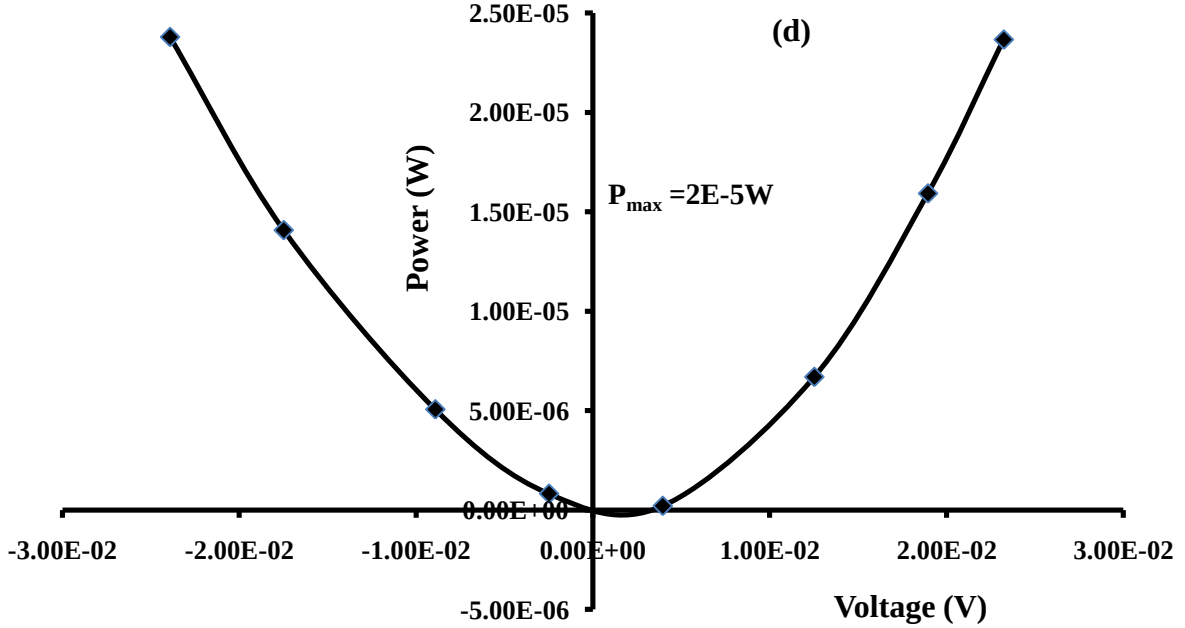
(d)
Power (W)
2.50E-05
2.00E-05
1.50E-05
1.00E-05
5.00E-06
0.00E+00
-5.00E-06
P_{max} =2E-5W
-3.00E-02
-2.00E-02
-1.00E-02
0.00E+00
1.00E-02
2.00E-02
3.00E-02
Voltage (V)

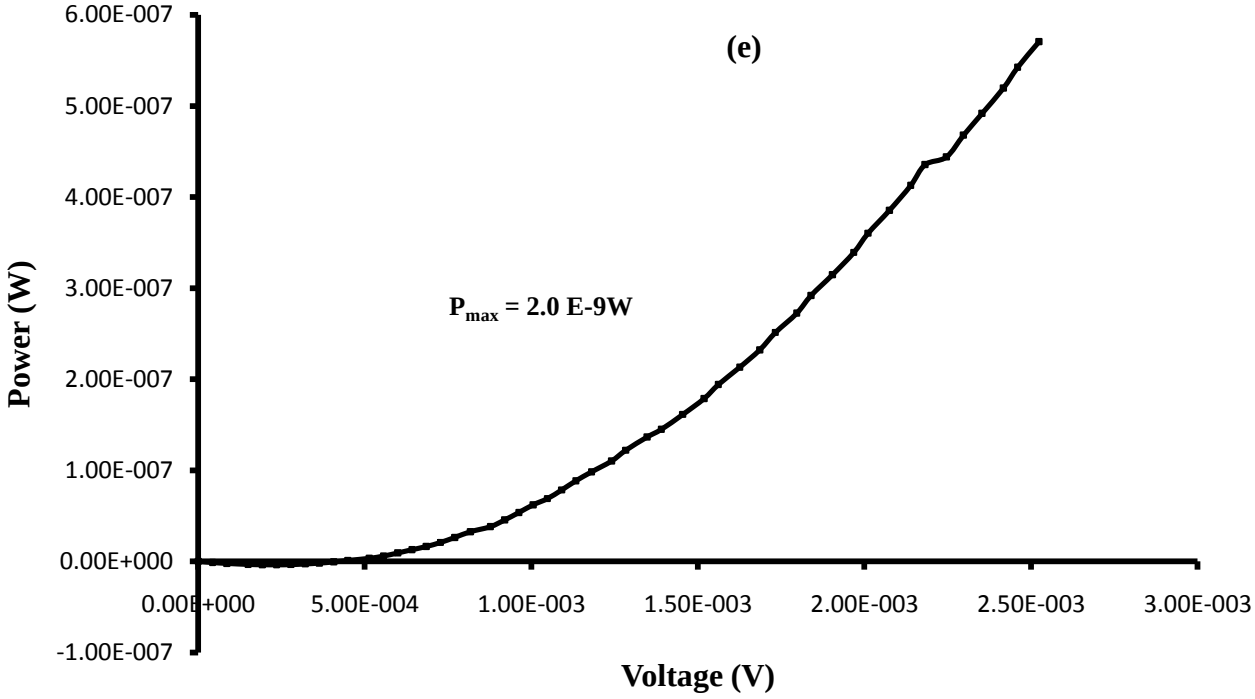

Figure 4.9: Power-Voltage Curves of the Devices Made from Active Layer Annealed at: (a) RT (b) 50^{o}C (c) 100^{o}C (d) 150^{o}C (e) 200^{o}C

Table 4.1: Summary of Electrical Characteristics Parameters

Annealing Temperature (^{0}C)	Open Circuit Voltage (Voc) (V)	Short Circuit Current (Isc) (A)	Maximum Power Point (Pmax) W	Fill Factor FF
RT	1.25 E-2	5.0 E-4	1.16 E-6	0.18
50	3.8 E-2	1.002 E-3	1.08 E -5	0.28
100	1.92 E-2	1.003 E-3	5.0 E-6	0.26
150	3.8 E-3	2.0 E-4	2.0 E-7	0.26
200	4.06 E-4	3.42 E-5	2.0 E-9	0.13

4.3.2 Effect of Annealing Temperature on V_{oc} and I_{sc} of the Devices

Figure 4.10 shows the effect of annealing temperature on short circuit current (I_{sc}) and open circuit voltage (V_{oc}). Both the I_{sc} and V_{oc} increase up to a peak with increase in annealing temperature from room temperature to about 80^{0}C and 55^{0}C respectively. Upon further increase in

annealing temperature, I_{sc} and V_{oc} drop drastically leading to the marked decrease in fill factor.

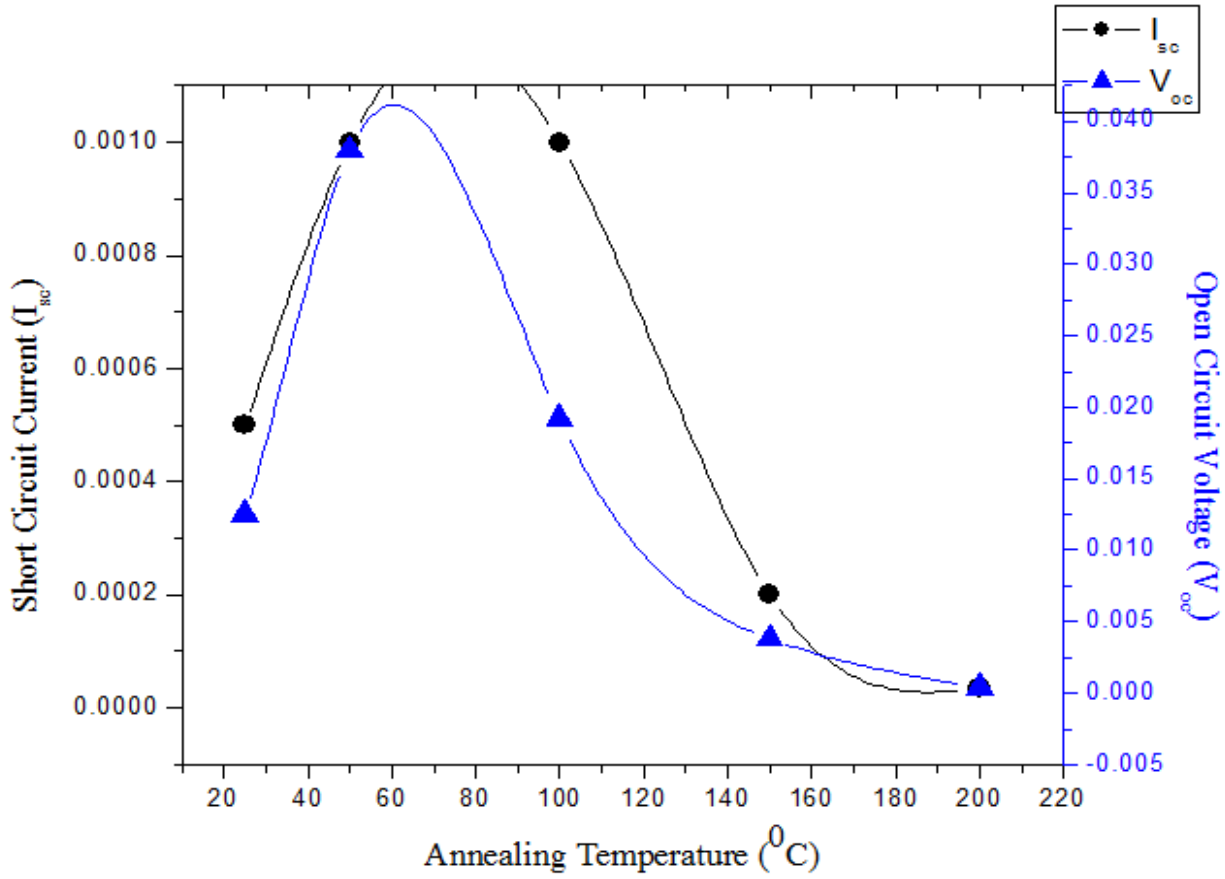

Figure 4.10: V_{oc} and I_{sc} versus Annealing Temperature of P3HT:PCBM

4.4 REFERENCES

[1]. Ji HyeJeon , HangKenLee , DongHwanWanga, JongHyeokPark, O OkPark: Solar Energy Materials & Solar Cells 102 (2012) 196–200

[2] C. Muller, A.Toby, M. Ferenczi, J. Frost, J. Nelson, Advance Materials, 20 3510 (2008)

CHAPTER 5

CONCLUSION AND SUGGESTIONS FOR FUTURE WORK

5.1 CONCLUSION

In this thesis, the various ways by which annealing treatment has affected both the optical and electrical properties as well as microstructures of P3HT:PCBM – based bulk heterojunction solar cells have been studied. The relationship between annealing temperature and device performance of P3HT:PCBM based organic solar cells has been studied. It has been shown that the morphology of the active layer can be controlled by thermal annealing. Careful control of the active layer by thermal annealing will result in a favourable phase segregation of P3HT and PCBM component as charge carrier dissociation. The charge transport through the blend is highly dependent on the arrangement of P3HT and PCBM as well as an increase in the interface between donor and acceptor. This improved interface was thought to have consequentially affected the fill factor. Short circuit current which is the main indicator of charge transport and photogeneration capabilities of an organic solar cell [1] is however more dependent on annealing temperature compared to the open circuit voltage as there was more increase in I_{sc} with increasing temperature.

Thermal annealing has been proved to increase the crystallinity of P3HT:PCBM films. The images show the presence of clusters of PCBM and this is believed to be as a result of strong phase separation. The needle-like PCBM aggregates that were observed at higher annealing temperatures was dependent on crystallization kinetics. Both the optical images and AFM images show that the surface roughness of the annealed films gets higher with increase in temperature from 50^0C to 100^0C then gets less rough at higher annealing temperature of 200^0C which also has an effect on the electrical properties of the devices that were made from them. Also the SEM images of the annealed active layers having different PCBM composition were presented and the blends with the largest amount of the PCBM did not allow the arrangement of P3HT polymer chains. Suitable

temperatures exist for which thermal annealing treatments of organic solar cells can be made leading to better performing systems.

Finally, the absorption spectrum equally exhibits a strong modification after annealing. The improvement in the absorptivity of the films can then attribute to the enhancement of carrier mobility in the polymer domains.

5.2 SUGGESTION FOR FUTURE WORK

More work needs to be done to vary process conditions like annealing times and temperatures to tailor the morphology of active layers as these parameters needs to be specifically optimized for better performing devices. Also post-production thermal annealing treatment should be carried out on fabricated devices as this may result in an improved performance as a result of improved contact between the active layer and the cathode.

5.3 REFERENCES

[1] D Chirvase, J Parisi1, J C Hummelen and V Dyakonov: Nanotechnology 15 (2004) 1317–1323